examined by dot blot analysis (Fig. 1C), which indicated that the binding capacity of the RNA pools was enriched in the earlier cycles of the selection. The RNA in pool 5 appeared to show the strongest binding to NS5B.

Individual RNA clones from pool 5 exhibited significantly stronger binding to NS5B compared to those from pool 0 ($P < 0.01$, Fig. 1D). The 9 highest binding mRNA 3′-UTR clones in pool 5 are listed in Table 1. The C5, NFS1 and RPL41 clones contained the 3′-end of the 3′-UTR sequences (Table 2), while the other 6 clones contained the full length 3′-UTR sequences plus the 3′-end of the coding sequences. A consensus RNA motif was not identified among these clones even using the computer program Nucleotide BLAST.

We analyzed the binding capacity of the 3′-UTR sequences from the pool 0 and 5 clones by gel mobility shift assay (Fig. 2A). Because these clones contained various lengths of the cDNA fragments under the T7 promoter, in this experiment, the 47-nucleotide RNA sequence just upstream of the 3′-end of each clone was synthesized and used in the gel mobility shift assay. The RNA-protein complexes appeared to form multiple bands, representing the oligomeric character of the NS5B protein (Lee et al., 2004). The pool 0 RNA 3′-UTRs exhibited relatively poor binding to NS5B. While the pool 5 clone RPS15A 3′-UTR exhibited poor binding, 5 out of 6 of the 3′-UTR sequences from pool 5 exhibited tighter binding than those from pool 0.

The 3′-UTRs of GAL-1 and RPS4X mRNA bind tightly to NS5B

We further analyzed two of the mRNA clones. GAL-1: lectin, galactoside-binding, soluble, 1 (LGALS1) mRNA encodes the galectin-1 protein, the expression level of which in HepG2 cells is known to be relatively low (Table 1). RPS4X: ribosomal protein S4, X-linked mRNA, is expressed at high level in a wide range of organs (Table 1, http://157.82.78.238/refexa/main_search.jsp). These two genes have relatively short 3′-UTRs (51 and 68 nucleotides, respectively), which we would make them suitable for further analysis. A gel mobility shift assay revealed that both the 3′-UTRs of GAL-1 mRNA and RPS4X mRNA formed a complex, not only with GST-NS5B, but also with NS5B and not GST (Fig. 2B and C), indicating specific binding of the RNA elements to NS5B. The secondary structure analysis by the mfold computer program (Zuker, 2003) indicated the presence of 2 stem-loop structures in the 3′-UTR of GAL-1 mRNA (Fig. 3A, GAL-1 1–51), while the 3′-UTR of RPS4X mRNA did not have any evident secondary structure and appeared to be single-stranded (Fig. 3C).

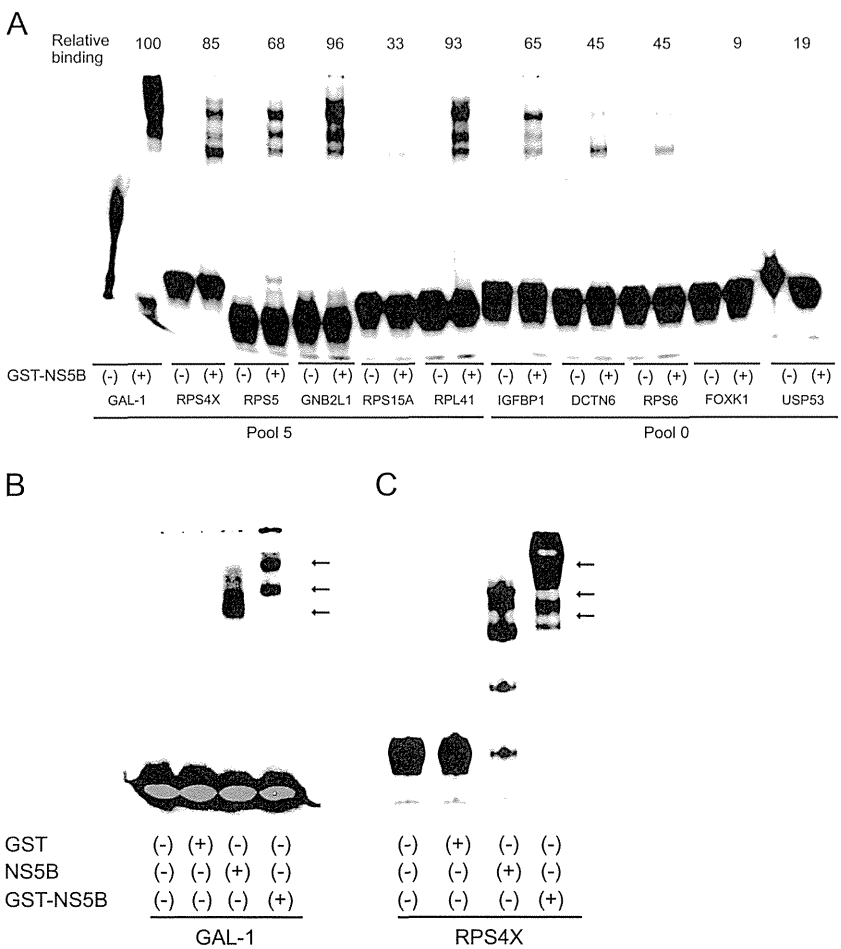

Fig. 2. RNA gel mobility shift assay using 3′-UTR mRNA sequences of the pool 0 and pool 5 clones. (A) An RNA segment (47-nucleotide length) just upstream of the 3′-end of each clone from pool 0 and pool 5 was synthesized, 5′-end labeled with 5′-[^{32}P] and incubated with (+) or without (−) GST-NS5B, and mixtures were run on a 5% polyacrylamide gel. The relative binding strength of each clone was determined by quantification by BAS2000 and is shown on the top portion of the gels. The binding strength of GAL-1 was set equal to 100. IGFBP1: insulin-like growth factor binding protein 1, DCTN6: dynactin 6, RPS6: ribosomal protein S6, FOXK1: forkhead box K1, USP53: ubiquitin specific peptidase 53. The specific interaction of the 3′-UTRs of GAL-1 and RPS4X mRNA with the NS5B protein is shown in panel B and C, respectively. GST, GST-truncated NS5BΔ21 (NS5B) or the GST-NS5BΔ21 (GST-NS5B) protein was incubated with either the GAL-1 (GAL-1 1–51, panel B) or RPS4X (RPS4X 1–68, panel C) RNA 3′-UTR as a probe and analyzed by RNA gel mobility shift assay. The arrows indicate the positions of the RNA-protein complexes.

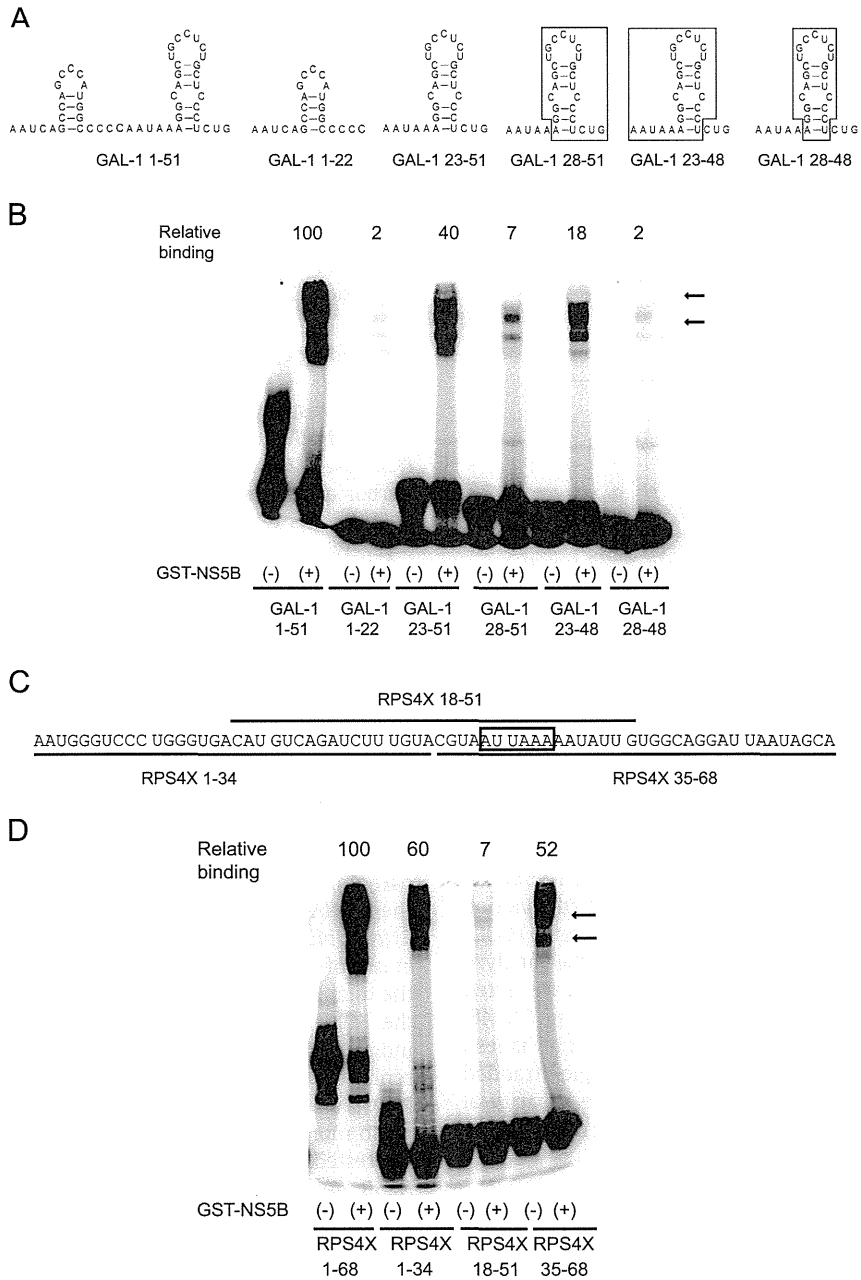

Fig. 3. *Analysis of the deletion mutants of GAL-1 and RPS4X mRNA 3′-UTRs by RNA gel mobility shift assay using the NS5B protein.* (A) *Predicted secondary structures of* GAL-1 1–51 and the deleted RNA clones (1–22, 23–51, 28–51, 23–48, and 28–48) by mfold computer analysis (Zuker, 2003) are shown. For GAL-1 28–51, 23–48 and 28–48, each secondary structure is shown in a box. (B) An RNA gel mobility shift assay using GAL-1 3′-UTR (1–51) and the deleted clones (1–22, 23-51, 28–51, 23–48 and 28–48). Chemically synthesized RNA was labeled with 5′-[^{32}P], incubated with (+) or without (−) GST-NS5B, and mixtures were run on a 5% polyacrylamide gel. (C) Nucleotide sequence of RPS4X 3′-UTR (1–68) RNA is shown. The 34 nucleotide RNA fragments (1–34, 18–51, 35–68) tested in panel D are indicated. The putative polyadenylation signal is boxed. (D) An RNA gel mobility shift assay using RPS4X 3′-UTR (1–68) and its deleted sequences (1–34, 18-51 and 35–68) in the presence (+) and absence (−) of the NS5B protein. The relative binding strength of each RNA molecule is shown at the top of the gels. The binding strength of GAL-1 1–51 (panel B) or RPS4X 1–68 (panel D) was set equal to 100. The arrows indicate the positions of the RNA-NS5B complexes.

Both the stem-loop structures and the single-strand regions of the GAL-1 3′-UTR are required for binding to NS5B

We undertook mapping of the NS5B binding sites on the 3′-UTRs of GAL-1 and RPS4X mRNA by testing the binding strength of the various portions of the 3′-UTR RNA segments by RNA gel mobility shift analysis, as shown in Fig. 3. Full length GAL-1 3′-UTR (GAL-1 1–51) RNA exhibited strong binding to NS5B (Fig. 3B). The 3′-half of the GAL-1 3′-UTR (GAL-1 23–51) exhibited weaker but still substantial binding, while the 5′-half (GAL-1 1–22) did not form a complex with NS5B. RPS4X 1–68 exhibited strong binding to NS5B. Both the 5′- (RPS4X 1–34) and the 3′-half (35–68) displayed weaker but still substantial levels of binding strength to NS5B (Fig. 3D). Interestingly, the middle portion of the RPS4X 3′-UTR (18–51) did not exhibit any binding to GST-NS5B. Because the nucleotide length of the 3 RPS4X RNA fragments tested were the same (34 nucleotides), the binding strength is not likely to be determined by the nucleotide length. The result instead indicates that either the 5′- or 3′- end of the 3′-UTR of RPS4X mRNA is indispensable for tight binding.

From the results of the GAL-1 mRNA binding, we thought that the stem-loop structure located on the 3′-half of the GAL-1 3′-UTR

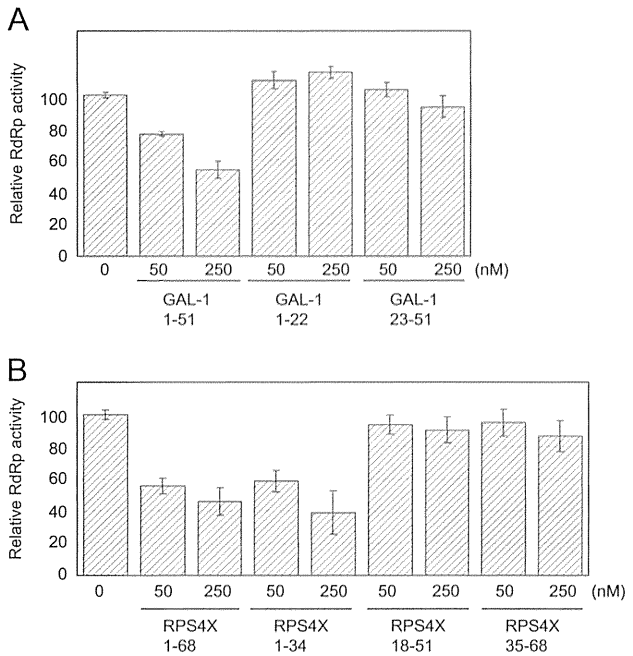

Fig. 4. Inhibition of RdRp activities by the mRNA 3′-UTRs. (A) GAL-1 mRNA or one of its deleted sequences (GAL-1 1–22 and 23–51, upper panel) was added in the poly(C)-oligo(G) RdRp reaction mixture (0, 50, and 250 nM) and the RdRp activity was measured. (B) The 3′-UTR of RPS4X mRNA or one of its deleted sequences (RPS4X 1–34, 18–51 and 35–68) was used as a competitor (0, 50, and 250 nM). The experiment was performed in triplicate. The standard deviations are shown by the error bars.

might be the key element in the tight binding of RNA to NS5B. The stem-loop structure is flanked by the 6-nucleotide polyadenylation signal (AAUAAA) on the 5′-end and the 3 nucleotide stretch (CUG) just upstream of the poly(A) tail on the 3′-end. To further analyze the binding of the GAL-1 3′-UTR RNA sequence to NS5B, we tested the deleted RNA oligonucleotides (GAL-1 28–51, 23–48 and 28–48, Fig. 3A) for the capacity to bind NS5B (Fig. 3B, right lanes). Interestingly, deletion of either of the flanking single-stranded nucleotides (GAL-1 28–51, 23–48) greatly reduced the capacity of the RNA to bind to NS5B. The stem-loop structure by itself (GAL-1 28-48) did not bind to NS5B.

mRNA 3′-UTRs with strong binding to NS5B inhibit the NS5B RdRp activity measured by poly(C)-oligo(G) system

The *in vitro* RdRp assay is a versatile assay that is used to evaluate the activity of the inhibitory factors against the NS5B polymerase (Kanamori et al., 2010). We used a primer-dependent RdRp system to evaluate the inhibitory effects of RNA segments from the 3′-UTRs of GAL-1 and RPS4X mRNA on NS5B RdRp. The full length 3′-UTRs of GAL-1 (GAL-1 1–51), RPS4X (RPS4X 1–68), or one of the dissected RNA fragments was added (50 or 250 nM) to the RdRp activity assay (Fig. 4). The full length 3′-UTRs of GAL-1 and RPS4X inhibited the RdRp activities efficiently. While RPS4X 1–34 also reduced the RdRp activity to 40% (Fig. 4B), none of the other dissected 3′-UTR RNA fragments (GAL-1 1–22, 23–51, RPS4X 18–51 or 35–68) inhibited the activity effectively.

The 3′–UTR sequences that bind to NS5B can serve as templates of NS5B RdRp

We tested whether the mRNA 3′-UTR molecules that exhibited potent binding to NS5B can serve as substrates of NS5B RdRp by adding RNA fragments to the NS5B RdRp reaction mixture (Fig. 5). In addition to pool 5 (GAL-1 and RPS4X) RNA molecules, pool 0 FOXK1 3′-UTR was very efficiently elongated when the poly (A) tail was present at the 3′-end (Fig. 5A).

Next, we tested whether the 3′-UTR sequence without the poly (A) tails can serve as a template for NS5B RdRp (Fig. 5B). The full length 3′-UTRs of GAL-1 (GAL-1 1–51) and RPS4X (RPS4X 1–68) appeared to be elongated by NS5B efficiently, while the 3′-end of FOXK1 3′-UTR, which is one of the pool 0 clones that displayed poor binding to NS5B (Fig. 2), was not elongated. In correlation with the binding ability (Fig. 3B), the 5′-portion of the GAL-1 3′-UTR (1–22) was elongated less efficiently compared with its 3′-portion (23–51).

The binding of GAL-1 and RPS4X mRNA to NS5B in vivo

To investigate whether the GAL-1 and RPS4X mRNA sequences bind to NS5B *in vivo*, we performed immunoprecipitation (IP)–RT-PCR assay (Fig. 6). RCYM1 cells are derived from Huh7 cells and harbor a genome-length dicistronic HCV genotype 1b full-length RNA. In this experiment, RCYM1 cells were cultured in a monolayer, where the viral proteins are efficiently produced while the viral particles are less efficiently secreted compared with those in three-dimensional culture (Murakami et al., 2006). A cytoplasmic extract of the monolayer-cultured RCYM1 cells was immunoprecipitated with a NS5B antibody in order to monitor the binding of RNA molecules to NS5B in the HCV replication complex by applying RT-PCR to the co-immunoprecipitated RNA molecules using specific primer pairs (Fig. 6A). Huh7 parental cells appeared to contain substantial amounts of the tested RNA molecules (Fig. 6A, GAL-1, RPS4X and FOXK1, Total RNA, Huh7). The RT-PCR product from GAL-1 as well as from RPS4X RNA was detected in the IP eluate of RCYM1 cells, while it was not detected in the parental Huh7 cell IP eluate, indicating the *in vivo* interaction of these RNA molecules with NS5B in the replication complex. FOXK1 RNA, which does not bind to NS5B, was not detected in the IP eluate of either RCYM1 cells or Huh7 cells, in spite of the fact that the total Huh7 cell RNA appears to contain a substantial amount of the FOXK1 RNA (Fig. 6A, FOXK1, Total RNA, Huh7). The results indicate that NS5B as well as other components in the HCV replication complex interact specifically with the GAL-1 and RPS4X RNA molecules.

To monitor the NS5B-RNA interaction *in vivo* more specifically, we tested COS cells transiently transfected with the FLAG-fused NS5B gene (Fig. 6B). The FLAG-fused NS5B protein from the cytoplasmic lysates of COS cells transfected with an NS5B expressing plasmid (pFLAG-5B) was immunoprecipitated with a FLAG antibody. RT-PCR was performed to monitor the specific binding of RNA molecules to NS5B. Non-transfected COS cells appeared to contain substantial amounts of the tested RNA molecules (Fig. 6B, GAL-1, RPS4X and FOXK1, Total RNA, Transfection (−)). The RT-PCR products from GAL-1 RNA and RPS4X RNA were detected in the IP eluate of COS cells expressing the NS5B protein (pFLAG-5B), while they were not detected in the mock–transfected COS cell IP eluate (pFLAG-CMV-4). In contrast, FOXK1 RNA, which does not bind to NS5B, was not detected in the IP eluate from the NB5B expressing COS cells (pFLAG-5B, FOXK1). These results indicate that the GAL-1 and RPS4X mRNA molecules directly interact with NS5B *in vivo*.

Discussion

We constructed a cDNA library that contained mostly 3′-UTR sequences from a human hepatoblasma cell line, HepG2. By using iterative selection cycles, we obtained 3′-UTR RNA segments that bind tightly to the HCV NS5B protein. In an earlier study by Gao et al. (1994), a similar cDNA library was constructed using a simpler method and 3′-UTR sequences were identified that bind

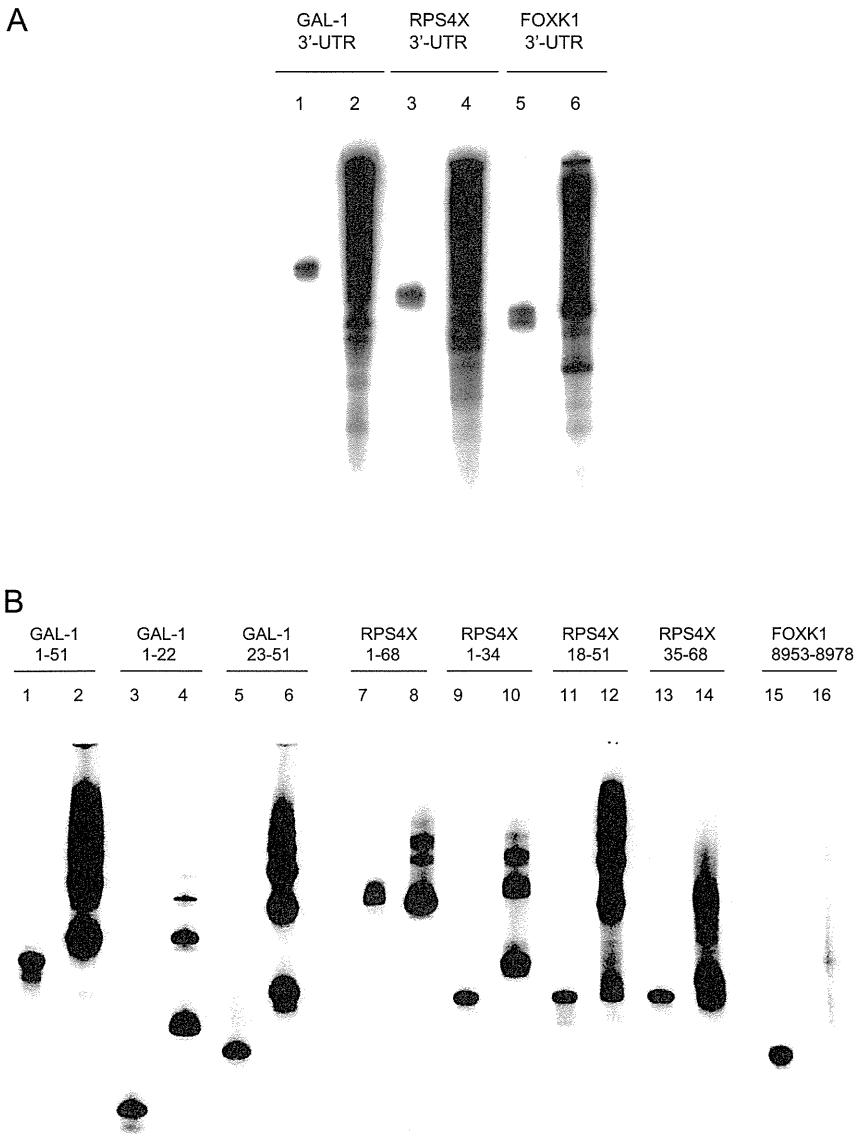

Fig. 5. RNA synthesis by NS5B RdRp using RNA 3′-UTR sequences as the templates. (A) The 3′-portion of GAL-1 (the 44-nucleotide coding, 51-nucleotide 3′-UTR and 26-nucleotide poly(A) tail), RPS4X (the 4-nucleotide coding, 64 nucleotide 3′-UTR and 24-nucleotide poly(A) tail) or FOXK1 (the 59-nucleotide 3′-UTR and 18-nucleotide poly (A) tail) mRNA segment was incubated with recombinant NS5B, cold NTPs and [α-^{32}P]UTP, and the RdRp products were analyzed by electrophoresis on a 12% polyacrylamide/ 7 M urea gel. For reference, the RNA templates were labeled at the 5′-end with [γ-^{32}P] by using T4 polynucleotide kinase and electrophoresed side-by-side with each RdRp product (lanes 1, 3 and 5). B. The 3′-UTR sequences without any poly(A) tails were tested similarly. The 3′-UTR of GAL-1 (GAL-1 1–51), its deleted form (GAL-1 1–22, 23–51), the 3′-UTR of RPS4X (RPS4X 1–68), its deleted form (RPS4X 1–34, 18–51, 35–68) or the FOXK1 3′-UTR segment (3′-end 26 nucleotides) was tested as a template for NS5B RdRp. For reference, the RNA templates were labeled at the 5′-end with [γ-^{32}P] using T4 polynucleotide kinase and electrophoresed side-by-side with each RdRp product (lanes 1, 3, 5, 7, 9, 11, 13 and 15).

to Hel-N1/Hel-N2 proteins. In the present study, by performing partial RNase T1 treatment of HepG2 RNA and size fractionation of cDNA fragments, we successfully removed approximately 99% of the coding sequences from the cDNA library. According to the UTR data base, approximately 50% of the 3′-UTRs of mRNA are less than 500 nucleotides (Grillo et al., 2010). Therefore, we decided to focus our attention on the shorter 3′-UTR sequences and recovered cDNA fragments 75–150 nucleotides in length, comprising approximately 9% of mRNA 3′-UTR sequences. As a result, 67.5% (27/40) of the clones in the library contained the 3′-end of the 3′-UTR (an average of 60.4 nucleotides) plus poly(A) tails and did not contain any coding regions. The rest of the pool 0 clones (13/40) contained the full length 3′-UTRs (an average of 47.5 nucleotides) and very short coding sequences (an average of 36.2 nucleotides) plus poly(A) tails.

The binding capacity of the RNA pool to NS5B increased as the selection cycles proceeded, reaching a peak at pool 5. Among the highest 9 binders in pool 5, 4 were housekeeping genes (Table 1). The frequency of these 9 high binding clones as a whole in the pool increased after the selection cycles (pool 5, 19/188, Table 2), while there were fewer in pool 0 (2/67), indicating the effectiveness of the selection process ($P < 0.05$).

Stem-loop structures have been considered to be important targets of RNA binding proteins (Dingwall et al., 1989; Koeller et al., 1989;

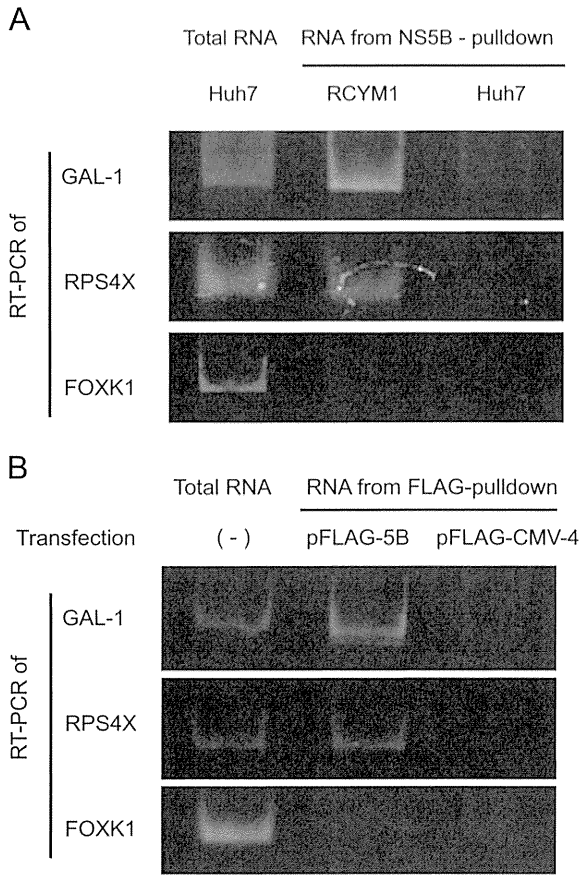

Fig. 6. The specific interaction of the NS5B protein with GAL-1 and RPS4X mRNA 3′-UTRs *in vivo*. (A) Immunoprecipitation using an anti-NS5B antibody was performed using cell extracts of RCYM1 cells or Huh7 cells. Following the RNA extraction of the immunoprecipitants, RT-PCR was performed using a primer pair specific for each mRNA to monitor GAL-1, RPS4X or FOXK1 mRNA bound to NS5B. As a reference, RT-PCR was carried out using total RNA from Huh7 cells (Total RNA) using the same primer pairs and the PCR products were run on 6% polyacrylamide gels side-by-side with the IP-RT-PCR products. (B) Immunoprecipitation using an anti-FLAG antibody was performed using cell extracts of COS cells transfected with either a FLAG-tag fused NS5B expression vector (pFLAG-5B) or a blank vector (pFLAG-CMV-4). RNA molecules bound to NS5B *in vivo* were amplified by RT-PCR and visualized as described in panel A. As a reference, RT-PCR was carried out using total RNA from nontransfected COS cells (Total, Transfection (–)) using the same primer pairs.

Munishkin et al., 1991; Tan et al., 1996; Nomaguchi et al., 2004; Kim et al., 2007). While the 3′-UTR of RPS4X mRNA is single-stranded and the full length 3′-UTR (68 nucleotides length) appears to be important for tight binding to NS5B, the stem-loop structure at the 3′-end of GAL-1 RNA also appears to be important for NS5B binding. Of note, the flanking 5′- and 3′-single-strand nucleotides were also indispensable for the tight binding to NS5B, having a similar property as the aptamers to NS5B reported in our earlier study (Kanamori et al., 2009).

GAL-1 1–51, as well as RPS4X 1–68 and 1–34 exhibited comparatively high affinity binding to NS5B in gel mobility shift analysis (Fig. 3), and at the same time strong inhibitory effects against RdRp activity (Fig. 4). The binding strength to NS5B was well correlated with the inhibitory effect on NS5B RdRp and also the efficiency as a template of NS5B RdRp in most of the RNA fragments we tested. RPS4X 18–51 exhibited weak binding to NS5B and weak inhibition on the RdRp, and yet was still efficiently elongated by NS5B RdRp. This suggests that tight binding is not necessarily required for the RNA molecules to interact with the NS5B RdRp catalytic site for replication. This result also suggests that there may be a population of mRNA molecules that did not survive the *in vitro* selection in this study but still can be elongated efficiently by NS5B RdRp.

Although limited to the three mRNA clones tested in this study, all of the RNA molecules bearing poly(A) tails on the 3′-ends were very efficiently elongated by NS5B, while the elongation efficiency of the 3′-UTRs without any poly(A) tails depended on their individual sequences (Fig. 5). The *in vivo* situation may be different because the poly(A) tails are likely to form complexes with other cellular factors such as the poly(A) binding protein and the poly (A) polymerase, and the importance of the poly(A) tail in the RdRp reaction should not be underestimated, while the 3′-UTR portions of mRNA appear to be more likely to interact with cellular or viral proteins.

We employed immunoprecipitation (IP)–RT-PCR and demonstrated that the GAL-1 and RPS4X mRNA 3′-UTR sequences actually do interact with NS5B *in vivo*. Notably, these mRNA molecules were shown to bind to NS5B in the replicon cell line RCYM1, where NS5B is one of the components of the HCV replication complex in the ER-derived membrane spherules, which are termed membranous web. The *in vivo* interaction of NS5B and these mRNA molecules suggests a mechanism by which the gene expression levels might be regulated by NS5B in HCV-infected cells. Compared to the abundant, constitutively-expressed housekeeping RPS4X gene product (Eisenberg and Levanon, 2003), the regulation of the gene expression of GAL-1 is biologically of greater importance, as the expression level of the GAL-1 gene is relatively low in the liver (Camby et al., 2006). In the COS cell experiment, where only NS5B was expressed transiently (Fig. 6B), the *in vivo* interaction of these RNA molecules with NS5B was shown to probably occur through a direct interaction with NS5B. The interaction of the NS5B protein with the GAL-1 mRNA 3′-UTR may influence the mRNA turnover rate and increase or decrease its expression level, since the control of the mRNA half life is considered to be regulated mainly by the 3′-UTR portions of the RNA (Ross 1995).

Although percentage of the immunoprecipitated GAL-1 and RPS4X mRNA was estimated to be as little as 0.1% of the total cellular mRNA molecules (Fig. 6), the *in vivo* interaction of NS5B with cellular mRNA may play a role in the host immune response against HCV infection. Generation of double stranded RNA molecules following the elongation of the host mRNA molecules by NS5B RdRp may increase the innate immunity against HCV infection (Ranjith-Kumar et al., 2011).

Recently, GAL-1 has received considerable attention because of its pleiotropic functions, such as promoting the apoptosis of activated T cells (Perillo et al., 1995; Matarrese et al., 2005), cytokine production (IL-5, IL-10, TGF-β), the regulation of CD4+ CD25+ T cells (Santucci et al., 2000; Garin et al., 2007), cell-extracellular matrix and cell-cell interaction, cell migration, angiogenesis, tumor-immune escape and correlation with tumor aggressiveness, especially hepatocellular carcinoma (Liu and Rabinovich, 2005; Rabinovich, 2005; Salatino et al., 2008; Spano et al., 2010). Thus, GAL-1 expression under a condition of viral infection may aid viral survival in the infected cells.

In the present study, we demonstrated that NS5B interacts with GAL-1 and RPS4X mRNA not only *in vitro* but also *in vivo* through the 3′-UTR portions. Further studies are required to elucidate how it is that NS5B-mRNA interactions modulate the expression of these genes.

In conclusion, we have identified a population of liver cellular mRNA that binds to the NS5B protein through the 3′-UTR regions by employing an iterative selection cycle using an mRNA library enriched with the 3′-UTR portions. Elucidating the interaction of the cellular mRNA 3′-UTRs and HCV NS5B RdRp will be a great help for understanding the mechanism by which HCV replicates in the intracellular environment in association with cellular factors.

Materials and methods

Purification of the recombinant NS5B protein

A recombinant glutathione *S*-transferase (GST)–NS5B (strain BK, genotype 1b) fusion protein that lacks the C-terminal 21 amino acids portion was produced and purified as described (Uchiyama et al., 2002). Purification of the GST-free NS5B protein was performed as described in our previous work (Kanamori et al., 2009). The protein concentration was measured by Coomassie staining or the Bradford method.

Preparation of a 3′-UTR cDNA library

Total RNA was extracted from HepG2 cells with TRIzol (Invitrogen) and partially digested with 0.01 U/ml RNase T1 (Ambion) at room temperature for 15 min. The mRNA 3′-UTR fragment was obtained using the PolyATract mRNA isolation system (Roche) and reverse transcribed with a cDNA library construction kit (Takara). Subsequently, cDNA was size fractionated by polyacrylamide gel electrophoresis to obtain the 3′-cDNA fragments sizing from 75 to 150 base pairs. The recovered cDNA fragments were digested by EcoRI and NotI, and subcloned into the pAP3neo pre-digested vector (Takara). Plasmids containing cDNA clones were linearized by NotI and an RNA pool was synthesized (pool 0) using T7 RNA polymerase.

Selection procedure

Approximately 10^5 individual RNA molecules were used as the initial RNA pool (pool 0) for selecting the cellular RNA 3′-UTRs that bind tightly to the HCV NS5B protein. A 100 μg of the GST-NS5B protein was incubated with 200 μl of glutathione agarose beads (Sigma) in 2 ml of LG buffer (2 mM Tris–HCl [pH 7.5], 1 mM EDTA, 5 mM DTT, 0.5% Triton X-100, 0.2 mM PMSF and 40% glycerol) containing 150 mM NaCl for 1 h at 4 °C. Following incubation, the beads were washed 5 times with LG buffer containing 150 mM NaCl to remove any unbound protein, and subsequently washed 5 times with binding buffer (8 mM Hepes [pH 7.9], 40 mM NaCl, 2 mM EDTA, 0.2 mM DTT, 0.2 mM PMSF and 1.6% glycerol). The initial pool of RNA was added to the beads and allowed to bind for 15 min at 30 °C in 800 μl of binding buffer containing 50 μg/ml tRNA. After 5 washes with the binding buffer, the RNA molecules that remained bound to the beads were eluted by incubation with 300 μl of proteinase K digestion buffer (20 mM Tris–HCl [pH 7.9], 100 mM NaCl, 10 mM EDTA, 1% SDS and 400 μg/ml proteinase K) for 30 min at 37 °C. RNA was extracted with phenol/chloroform and precipitated with ethanol. The recovered RNA was reverse transcribed using primer A (5′-TAATACGACTCACTATAGGGAATTCCCGGG-3′) and PCR-amplified (25 cycles; 30 s at 96 °C, 30 s at 55 °C, 45 s at 72 °C) by adding primer B (5′-ACGTGCGGCCGCTTTTTTTTT-3′). Primers were removed from the reaction mixture with a Micro Bio-Spin 30 Chromatography Column (Bio-Rad). The recovered PCR products were used as templates to synthesize an RNA pool (pool 1).

Selection cycles were repeated until we obtained the pool 8 RNA. For the selection cycles 2–7, 25 μg of GST-NS5B and 50 μl of glutathione agarose were used. For the selection cycles 3–7, RNA pools were first absorbed to GST-attached glutathione agarose beads to remove RNA molecules that were bound to the GST or agarose beads, and the unbound RNA was used for the selection process.

Filter binding assay and RNA gel mobility shift experiments

Filter binding assay was used as described previously to measure the binding strength of each RNA molecule to NS5B (Kanamori et al., 2009).

For RNA gel mobility shift analysis, synthetic RNA molecules were labeled with ^{32}P at the 5′-end using T4 polynucleotide kinase and [γ-^{32}P]ATP. The labeled RNA probes were purified by denaturing gel electrophoresis and subsequently incubated with proteins in a total of 10 μl of binding buffer containing 50 μg/ml tRNA for 20 min at 22 °C. The samples were loaded on a 6% polyacrylamide gel in a 1:4 dilution of Tris-borate/EDTA buffer and electrophoresed at 300 V and 4 °C. Gels were visualized with a Bioimage Analyzer BAS2000.

RdRp assay

For competition experiments, RdRp activity was measured by using the poly(C)-oligo(G) system, as previously described (Uchiyama et al., 2002). Reactions were performed in a 100-μl reaction mixture containing 20 mM Tris–HCl (pH 7.5), 25 mM KCl, 1 mM DTT, 5 mM $MnCl_2$, 0.01% BSA, 100 U/ml RNasin, 5 μg/ml actinomycin D, 0.4 μCi [^{3}H]GTP, 0.5 μg/ml poly(C), 50 nM oligo $(rG)_{12}$ and 80 nM purified NS5B in the presence (50 or 250 nM) or absence of competitor RNA molecules. After incubation for 2 h at room temperature, samples were precipitated with 3 volumes of ethanol in the presence of 10 μl of 3 M sodium acetate (pH 5.2) and 3 μl of ethachinmate (Nippon Gene), and transferred to GF/C glass microfiber filters (Whatman). The filters were rinsed with 70% ethanol and air dried. The filter bound radioactivity was measured using a scintillation counter. Experiments were performed in triplicate and the standard deviations are indicated in Fig. 4.

GAL-1 or RPS4X 3′-UTR mRNA was used as the template for RNA synthesis. RNA templates (final concentration of 125 nM) were incubated with 80 nM recombinant GST-NS5B in a 100-μl reaction mixture containing 50 mM Tris–HCl (pH 8), 50 mM NaCl, 100 mM KCl, 5 mM $MnCl_2$, 1 mM DTT, 20 μg/ml actinomycin D, 20 U RNasin, 10% glycerol, 0.5 mM each rATP, rCTP, rGTP and 5 μM rUTP with 40 μCi [α-^{32}P]UTP (10 mCi/ml) for 2 h at 25 °C. Reaction products were extracted with phenol/chloroform, precipitated with ethanol and 3 M sodium acetate, purified with Centri-Sep spin columns (Life Technologies), denatured in 95% formamide, and separated on a 6% polyacrylamide/8 M urea gel.

Immunoprecipitation-reverse transcription-PCR (IP-RT-PCR)

COS cells were maintained in Dulbecco's modified Eagle's medium supplemented with 10% fetal bovine serum. RCYM1 is a Huh7 derived cell line and was a generous gift from Dr. Takeya Tsutsumi (The University of Tokyo) (Murakami et al., 2006). RCYM1 cells harbor a genome-length dicistronic HCV genotype 1b full-length RNA and were cultured in a monolayer in Dulbecco's modified Eagle's medium with 10% fetal bovine serum and 0.5 mg/ml G418 and harvested at the exponential growth phase.

We constructed a FLAG-NS5B expressing plasmid, pFLAG-5B to express the NS5B protein in COS cells. The NS5B coding region cDNA lacking the C-terminal 21 amino acid portion was PCR amplified using the primer C (5′-AAGAATGCGGCCGCGTCAATGTCCTACACA-3′) and primer D (5′-CCGGAATTCTTAACGGGGTCGGGCACG-3′), with the pGEX-4T-2-5bC21 plasmid as the template (Uchiyama et al., 2002). Following digestion with EcoRI and NotI, the DNA fragment was ligated into the pFLAG-CMV-4 vector (Sigma) to obtain the pFLAG-5B plasmid. The pFLAG-5B expression plasmid was transiently transfected into COS cells using Lipofectamine™ LTX (Invitrogen). Cells were incubated 24 h at 37 °C in a CO_2 incubator before harvesting for the analysis.

Cytoplasmic extracts of transfected COS cells containing the FLAG-fused NS5B protein were collected using the FLAG® Immunoprecipitation Kit (Sigma) by following the manufacturer's instructions. Expression of the FLAG-NS5B fusion protein was

confirmed by Western blotting using anti FLAG-M2 (Sigma) and anti-HepC-NS5b (Santa Cruz Biotechnology) antibodies.

For RCYM1 cells, after preparing the cytoplasmic extract, immunoprecipitation was carried out using the anti-HepC-NS5b (Santa Cruz Biotechnology) antibody.

The eluates from the immunoprecipitation were treated with proteinase K to release the NS5B-bound RNA molecules. RNA was isolated using TRIzol reagent (Invitrogen) as instructed by the manufacturer, followed by DNase treatment to completely remove the cellular genomic DNA. For detecting mRNA molecules bound to NS5B, RT-PCR was performed using gene-specific primer pairs for GAL-1 (5′-GGACCGAGCAGCGGGAGG-3′ and 5′-CAGGGGAGCAGAGG-CAGC-3′; a 250-bp product; annealing temperature: 61 °C), RPS4X (5′-CGACTTTCCAACATTTTT-3′ and 5′-TGCTATTAATCCTGCCAC-3′; a 200-bp product; annealing temperature: 52 °C) or FOXK1 (5′-CGCG-GCGGCCTGTGGGCA-3′ and 5′-TGCGTTTCTGTCTGTCCT-3′; a 300-bp product; annealing temperature: 61 °C), respectively. The primer pairs for GAL-1 and RPS4X were designed to amplify the full length 3′-UTRs plus the 3′-end coding sequences, respectively, while the one for FOXK1 was designed to amplify the segment within the 3′-UTR of FOXK1. The PCR products were electrophoresed on 5% polyacrylamide gels and stained with ethidium bromide.

Acknowledgments

We would like to thank Prof. H. Aburatani at the Genome Science Division, Research Center for Advanced Science and Technology, The University of Tokyo for helpful discussion. We also thank S. Kawanabe for technical support.

This work was supported by New Energy and Industrial Technology Development Organization (NEDO) and carried out in cooperation with Japan Biochemistry Association (JBA).

References

Ago, H., Adachi, T., Yoshida, A., Yamamoto, M., Habuka, N., Yatsunami, K., Miyano, M., 1999. Crystal structure of the RNA-dependent RNA polymerase of hepatitis C virus. Structure 7, 1417–1426.

Antic, D., Lu, N., Keene, J.D., 1999. ELAV tumor antigen, Hel-N1, increases translation of neurofilament M mRNA and induces formation of neurites in human teratocarcinoma cells. Genes Dev. 13, 449–461.

Behrens, S.E., Tomei, L., De Francesco, R., 1996. Identification and properties of the RNA-dependent RNA polymerase of hepatitis C virus. EMBO J 15, 12–22.

Biroccio, A., Hamm, J., Incitti, I., De Francesco, R., Tomei, L., 2002. Selection of RNA aptamers that are specific and high-affinity ligands of the hepatitis C virus RNA-dependent RNA polymerase. J. Virol. 76, 3688–3696.

Blackham, S., Baillie, A., Al-Hababi, F., Remlinger, K., You, S., Hamatake, R., McGarvey, M.J., 2010. Gene expression profiling indicates the roles of host oxidative stress, apoptosis, lipid metabolism, and intracellular transport genes in the replication of hepatitis C virus. J. Virol. 84, 5404–5414.

Bressanelli, S., Tomei, L., Roussel, A., Incitti, I., Vitale, R.L., Mathieu, M., De Francesco, R., Rey, F.A., 1999. Crystal structure of the RNA-dependent RNA polymerase of hepatitis C virus. Proc. Natl. Acad. Sci. U.S.A. 96, 13034–13039.

Camby, I., Le Mercier, M., Lefranc, F., Kiss, R., 2006. Galectin-1: a small protein with major functions. Glycobiology 16, 137R–157R.

Cheng, J.C., Chang, M.F., Chang, S.C., 1999. Specific interaction between the hepatitis C virus NS5B RNA polymerase and the 3′ end of the viral RNA. J. Virol. 73, 7044–7049.

Choo, Q.L., Kuo, G., Weiner, A.J., Overby, L.R., Bradley, D.W., Houghton, M., 1989. Isolation of a cDNA clone derived from a blood-borne non-A, non-B viral hepatitis genome. Science 244, 359–362.

De Francesco, R., 1999. Molecular virology of the hepatitis C virus. J. Hepatol. 31 (Suppl. 1), 47–53.

Dingwall, C., Ernberg, I., Gait, M.J., Green, S.M., Heaphy, S., Karn, J., Lowe, A.D., Singh, M., Skinner, M.A., Valerio, R., 1989. Human immunodeficiency virus 1 tat protein binds trans-activation-responsive region (TAR) RNA in vitro. Proc. Natl. Acad. Sci. U.S.A. 86, 6925–6929.

Eckart, M.R., Selby, M., Masiarz, F., Lee, C., Berger, K., Crawford, K., Kuo, C., Kuo, G., Houghton, M., Choo, Q.L., 1993. The hepatitis C virus encodes a serine protease involved in processing of the putative nonstructural proteins from the viral polyprotein precursor. Biochem. Biophys. Res. Commun. 192, 399–406.

Eisenberg, E., Levanon, E.Y., 2003. Human housekeeping genes are compact. Trends Genet. 19, 362–365.

Friebe, P., Boudet, J., Simorre, J.P., Bartenschlager, R., 2005. Kissing-loop interaction in the 3′ end of the hepatitis C virus genome essential for RNA replication. J. Virol. 79, 380–392.

Gao, F.B., Carson, C.C., Levine, T., Keene, J.D., 1994. Selection of a subset of mRNAs from combinatorial 3′ untranslated region libraries using neuronal RNA-binding protein Hel-N1. Proc. Natl. Acad. Sci. U.S.A. 91, 11207–11211.

Garin, M.I., Chu, C.C., Golshayan, D., Cernuda-Morollon, E., Wait, R., Lechler, R.I., 2007. Galectin-1: a key effector of regulation mediated by CD4+CD25+ T cells. Blood 109, 2058–2065.

Grakoui, A., McCourt, D.W., Wychowski, C., Feinstone, S.M., Rice, C.M., 1993. A second hepatitis C virus-encoded proteinase. Proc. Natl. Acad. Sci. U.S.A. 90, 10583–10587.

Grillo, G., Turi, A., Licciulli, F., Mignone, F., Liuni, S., Banfi, S., Gennarino, V.A., Horner, D.S., Pavesi, G., Picardi, E., Pesole, G., 2010. UTRdb and UTRsite (RELEASE 2010): a collection of sequences and regulatory motifs of the untranslated regions of eukaryotic mRNAs. Nucleic Acids Res. 38, D75–80.

Guo, J., Yan, R., Xu, G.D., Zheng, C.Y., 2012. HCV NS5A and NS5B enhance expression of human ceramide glucosyltransferase gene. Virol. Sin. 27, 38–47.

Imai, T., Tokunaga, A., Yoshida, T., Hashimoto, M., Mikoshiba, K., Weinmaster, G., Nakafuku, M., Okano, H., 2001. The neural RNA-binding protein Musashi1 translationally regulates mammalian numb gene expression by interacting with its mRNA. Mol. Cell. Biol. 21, 3888–3900.

Kanamori, H., Yuhashi, K., Uchiyama, Y., Kodama, T., Ohnishi, S., 2009. In vitro selection of RNA aptamers that bind the RNA-dependent RNA polymerase of hepatitis C virus: a possible role of GC-rich RNA motifs in NS5B binding. Virology 388, 91–102.

Kanamori, H., Yuhashi, K., Ohnishi, S., Koike, K., Kodama, T., 2010. RNA-dependent RNA polymerase of hepatitis C virus binds to its coding region RNA stem-loop structure, 5BSL3.2, and its negative strand. J. Gen. Virol. 91, 1207–1212.

Kao, C.C., Yang, X., Kline, A., Wang, Q.M., Barket, D., Heinz, B.A., 2000. Template requirements for RNA synthesis by a recombinant hepatitis C virus RNA-dependent RNA polymerase. J. Virol. 74, 11121–11128.

Kato, N., Hijikata, M., Ootsuyama, Y., Nakagawa, M., Ohkoshi, S., Sugimura, T., Shimotohno, K., 1990. Molecular cloning of the human hepatitis C virus genome from Japanese patients with non-A, non-B hepatitis. Proc. Natl. Acad. Sci. U.S.A. 87, 9524–9528.

Kim, M., Kim, H., Cho, S.P., Min, M.K., 2002. Template requirements for de novo RNA synthesis by hepatitis C virus nonstructural protein 5B polymerase on the viral X RNA. J. Virol. 76, 6944–6956.

Kim, Y.G., Yoo, J.S., Kim, J.H., Kim, C.M., Oh, J.W., 2007. Biochemical characterization of a recombinant Japanese encephalitis virus RNA-dependent RNA polymerase. BMC Mol. Biol. 8, 59.

Koeller, D.M., Casey, J.L., Hentze, M.W., Gerhardt, E.M., Chan, L.N., Klausner, R.D., Harford, J.B., 1989. A cytosolic protein binds to structural elements within the iron regulatory region of the transferrin receptor mRNA. Proc. Natl. Acad. Sci. U.S.A. 86, 3574–3578.

Kolykhalov, A.A., Feinstone, S.M., Rice, C.M., 1996. Identification of a highly conserved sequence element at the 3′ terminus of hepatitis C virus genome RNA. J. Virol. 70, 3363–3371.

Lee, H., Shin, H., Wimmer, E., Paul, A.V., 2004. cis-acting RNA signals in the NS5B C-terminal coding sequence of the hepatitis C virus genome. J. Virol. 78, 10865–10877.

Lee, Y.J., Glaunsinger, B.A., 2009. Aberrant herpesvirus-induced polyadenylation correlates with cellular messenger RNA destruction. PLoS Biol 7, e1000107.

Lesburg, C.A., Cable, M.B., Ferrari, E., Hong, Z., Mannarino, A.F., Weber, P.C., 1999. Crystal structure of the RNA-dependent RNA polymerase from hepatitis C virus reveals a fully encircled active site. Nat. Struct. Biol. 6, 937–943.

Levine, T.D., Gao, F., King, P.H., Andrews, L.G., Keene, J.D., 1993. Hel-N1: an autoimmune RNA-binding protein with specificity for 3′ uridylate-rich untranslated regions of growth factor mRNAs. Mol. Cell. Biol. 13, 3494–3504.

Lin, C., Lindenbach, B.D., Pragai, B.M., McCourt, D.W., Rice, C.M., 1994. Processing in the hepatitis C virus E2-NS2 region: identification of p7 and two distinct E2-specific products with different C termini. J. Virol. 68, 5063–5073.

Liu, F.T., Rabinovich, G.A., 2005. Galectins as modulators of tumour progression. Nat. Rev. Cancer 5, 29–41.

Lohmann, V., Korner, F., Herian, U., Bartenschlager, R., 1997. Biochemical properties of hepatitis C virus NS5B RNA-dependent RNA polymerase and identification of amino acid sequence motifs essential for enzymatic activity. J. Virol. 71, 8416–8428.

Luo, G., Hamatake, R.K., Mathis, D.M., Racela, J., Rigat, K.L., Lemm, J., Colonno, R.J., 2000. De novo initiation of RNA synthesis by the RNA-dependent RNA polymerase (NS5B) of hepatitis C virus. J. Virol. 74, 851–863.

Matarrese, P., Tinari, A., Mormone, E., Bianco, G.A., Toscano, M.A., Ascione, B., Rabinovich, G.A., Malorni, W., 2005. Galectin-1 sensitizes resting human T lymphocytes to Fas (CD95)-mediated cell death via mitochondrial hyperpolarization, budding, and fission. J. Biol. Chem. 280, 6969–6985.

McCarthy, J.E., Kollmus, H., 1995. Cytoplasmic mRNA-protein interactions in eukaryotic gene expression. Trends Biochem. Sci. 20, 191–197.

Munishkin, A.V., Voronin, L.A., Ugarov, V.I., Bondareva, L.A., Chetverina, H.V., Chetverin, A.B., 1991. Efficient templates for Q beta replicase are formed by recombination from heterologous sequences. J. Mol. Biol. 221, 463–472.

Murakami, K., Ishii, K., Ishihara, Y., Yoshizaki, S., Tanaka, K., Gotoh, Y., Aizaki, H., Kohara, M., Yoshioka, H., Mori, Y., Manabe, N., Shoji, I., Sata, T., Bartenschlager, R., Matsuura, Y., Miyamura, T., Suzuki, T., 2006. Production of infectious hepatitis C virus particles in three-dimensional cultures of the cell line carrying the genome-length dicistronic viral RNA of genotype 1b. Virology 351, 381–392.

Nomaguchi, M., Teramoto, T., Yu, L., Markoff, L., Padmanabhan, R., 2004. Requirements for West Nile virus (−)- and (+)-strand subgenomic RNA synthesis in vitro by the viral RNA-dependent RNA polymerase expressed in *Escherichia coli*. J. Biol. Chem. 279, 12141–12151.

Oh, J.W., Sheu, G.T., Lai, M.M., 2000. Template requirement and initiation site selection by hepatitis C virus polymerase on a minimal viral RNA template. J. Biol. Chem. 275, 17710–17717.

Parrish, S., Resch, W., Moss, B., 2007. Vaccinia virus D10 protein has mRNA decapping activity, providing a mechanism for control of host and viral gene expression. Proc. Natl. Acad. Sci. U.S.A. 104, 2139–2144.

Perillo, N.L., Pace, K.E., Seilhamer, J.J., Baum, L.G., 1995. Apoptosis of T cells mediated by galectin-1. Nature 378, 736–739.

Poenisch, M., Bartenschlager, R., 2010. New insights into structure and replication of the hepatitis C virus and clinical implications. Semin. Liver Dis. 30, 333–347.

Rabinovich, G.A., 2005. Galectin-1 as a potential cancer target. Br. J. Cancer 92, 1188–1192.

Ranjith-Kumar, C.T., Wen, Y., Baxter, N., Bhardwaj, K., Cheng Kao, C., 2011. A cell-based assay for RNA synthesis by the HCV polymerase reveals new insights on mechanism of polymerase inhibitors and modulation by NS5A. PloS One 6, e22575.

Romero-Lopez, C., Berzal-Herranz, A., 2009. A long-range RNA-RNA interaction between the 5′ and 3′ ends of the HCV genome. RNA 15, 1740–1752.

Ross, J., 1995. mRNA stability in mammalian cells. Microbiol. Rev. 59, 423–450.

Salatino, M., Croci, D.O., Bianco, G.A., Ilarregui, J.M., Toscano, M.A., Rabinovich, G.A., 2008. Galectin-1 as a potential therapeutic target in autoimmune disorders and cancer. Expert Opin. Biol. Ther. 8, 45–57.

Santucci, L., Fiorucci, S., Cammilleri, F., Servillo, G., Federici, B., Morelli, A., 2000. Galectin-1 exerts immunomodulatory and protective effects on concanavalin A-induced hepatitis in mice. Hepatology 31, 399–406.

Spano, D., Russo, R., Di Maso, V., Rosso, N., Terracciano, L.M., Roncalli, M., Tornillo, L., Capasso, M., Tiribelli, C., Iolascon, A., 2010. Galectin-1 and its involvement in hepatocellular carcinoma aggressiveness. Mol. Med. 16, 102–115.

Takamizawa, A., Mori, C., Fuke, I., Manabe, S., Murakami, S., Fujita, J., Onishi, E., Andoh, T., Yoshida, I., Okayama, H., 1991. Structure and organization of the hepatitis C virus genome isolated from human carriers. J. Virol. 65, 1105–1113.

Tan, B.H., Fu, J., Sugrue, R.J., Yap, E.H., Chan, Y.C., Tan, Y.H., 1996. Recombinant dengue type 1 virus NS5 protein expressed in *Escherichia coli* exhibits RNA-dependent RNA polymerase activity. Virology 216, 317–325.

Tanaka, T., Kato, N., Cho, M.J., Shimotohno, K., 1995. A novel sequence found at the 3′ terminus of hepatitis C virus genome. Biochem. Biophys. Res. Commun. 215, 744749.

Uchiyama, Y., Huang, Y., Kanamori, H., Uchida, M., Doi, T., Takamizawa, A., Hamakubo, T., Kodama, T., 2002. Measurement of HCV RdRp activity with C-terminal 21 aa truncated NS5b protein: optimization of assay conditions. Hepatol. Res. 23, 90–97.

Vo, N.V., Oh, J.W., Lai, M.M., 2003. Identification of RNA ligands that bind hepatitis C virus polymerase selectively and inhibit its RNA synthesis from the natural viral RNA templates. Virology 307, 301–316.

Warner, J.R., Knopf, P.M., Rich, A., 1963. A multiple ribosomal structure in protein synthesis. Proc. Natl. Acad. Sci. U.S.A. 49, 122–129.

Yamada, N., Tanihara, K., Takada, A., Yorihuzi, T., Tsutsumi, M., Shimomura, H., Tsuji, T., Date, T., 1996. Genetic organization and diversity of the 3′ noncoding region of the hepatitis C virus genome. Virology 223, 255–261.

Zuker, M., 2003. Mfold web server for nucleic acid folding and hybridization prediction. Nucleic Acids Res. 31, 3406–3415.

Hepatology Research

Hepatology Research 2013; 43: 1005–1012 doi: 10.1111/hepr.12061

Original Article

Perihepatic lymph node enlargement is a negative predictor for sustained responses to pegylated interferon-α and ribavirin therapy for Japanese patients infected with hepatitis C virus genotype 1

Hiromi Hikita,[1]* Kenichiro Enooku,[1,2]* Yumiko Satoh,[1] Haruhiko Yoshida,[2] Hayato Nakagawa,[1,2] Ryota Masuzaki,[2] Ryosuke Tateishi,[2] Yoko Soroida,[1] Mamiko Sato,[1] Atsushi Suzuki,[1] Hiroaki Gotoh,[1] Tomomi Iwai,[1] Hiromitsu Yokota,[1] Kazuhiko Koike,[2] Yutaka Yatomi[1] and Hitoshi Ikeda[1,2]

Departments of [1]Clinical Laboratory Medicine and [2]Gastroenterology, Graduate School of Medicine, The University of Tokyo, Tokyo, Japan

Aim: Although perihepatic lymph node enlargement (PLNE) is reportedly associated with the negative outcome of interferon therapy for chronic hepatitis C, there were limitations in that the results were obtained in patients with various genotypes, viral loads and treatment regimens. We aimed to precisely clarify the significance of PLNE in interferon therapy for chronic hepatitis C.

Methods: Between December 2004 and June 2005, 112 patients with hepatitis C virus (HCV) genotype 1 and HCV RNA of more than 100 KIU/mL were enrolled, who underwent pegylated interferon-α plus ribavirin therapy thereafter. PLNE was defined as a perihepatic lymph node of more than 1 cm in the longest axis by ultrasonography.

Results: The sustained virological response (SVR) rate was lower in patients with PLNE (4/22, 18.2%) than in those without (37/90, 41.1%; $P = 0.045$) and viral load decline was smaller in patients with PLNE than in those without ($P = 0.028$). The proportion of PLNE positive patients was the smallest in the SVR group ($P = 0.033$) among the patient groups divided by the treatment outcome. PLNE was retained as a negative predictor for SVR by multivariate logistic regression analysis ($P = 0.012$). Furthermore, PLNE was not significantly associated with the mutations at HCV core protein and at interferon sensitivity-determining region, or interleukin-28B polymorphism in 45 patients with HCV genotype 1, enrolled between December 2011 and March 2012.

Conclusion: PLNE is a negative predictor for SVR in patients with HCV genotype 1 and HCV RNA of more than 100 KIU/mL treated with pegylated interferon-α plus ribavirin, independent of other known predictors for SVR.

Key words: chronic hepatitis C, hepatitis C virus core protein, interferon sensitivity-determining region, interleukin-28B

INTRODUCTION

PERIHEPATIC LYMPH NODE enlargement (PLNE) is frequently observed in patients with chronic liver disease,[1] especially in those with hepatitis C.[2,3] Although it has been shown that PLNE is associated with inflammatory activity, stage of liver fibrosis or hepatitis C viral load,[3–8] the reported findings were inconsistent,[2,9] suggesting that the clinical significance of PLNE has not been fully established yet. We have recently reported that PLNE is a negative predictor for hepatocellular carcinoma (HCC) development in chronic hepatitis C patients.[10]

Regarding PLNE and efficacy of interferon (IFN) therapy for chronic hepatitis C, PLNE was reportedly more frequently found in non-responders.[11,12] Dietrich *et al.* reported that perihepatic lymph node volume before IFN treatment was significantly larger in non-responders than in sustained virological responders,

Correspondence: Dr Hitoshi Ikeda, Department of Clinical Laboratory Medicine, Graduate School of Medicine, The University of Tokyo, 7-3-1 Hongo, Bunkyo-ku, Tokyo 113-8655, Japan.
Email: ikeda-1im@h.u-tokyo.ac.jp
*These authors contributed equally to this work.
Conflict of interest: none.
Received 9 November 2012; revision 10 December 2012; accepted 25 December 2012.

based on a study in which the patients had various genotypes and viral loads and were treated with IFN-α with or without ribavirin (RBV).[11] Soresi *et al.* reported that PLNE was more frequent in non-responders to IFN-α with RBV, although this association did not reach statistical significance by logistic regression analysis, in which the patients also had various genotypes.[12] We also reported that the sustained virological response (SVR) rate in patients who received IFN therapy was significantly lower in patients with PLNE than in those without, although our patients also had various genotypes and viral loads, and treatment regimens were various including IFN-α or pegylated IFN-α (PEG IFN) with or without RBV.[10] It is well known that patients with hepatitis C virus (HCV) genotype 1 and high baseline viral load are most difficult to treat with IFN[13] and that PEG IFN plus RBV has been the most effective standard of care for chronic hepatitis C until telaprevir emerged.[14] Thus, the previous results regarding PLNE and efficacy of IFN therapy for chronic hepatitis C had limitations, because they were analyzed with various genotypes, viral loads and treatment regimens.

In this study, in order to precisely clarify the potential association between PLNE and efficacy of IFN therapy for chronic hepatitis C, we analyzed the patients with HCV genotype 1 and HCV RNA of more than 100 KIU/mL at the start of therapy by PEG IFN with RBV in the well-characterized chronic hepatitis C cohort, in which liver stiffness values were found to be a risk for HCC development.[15]

METHODS

Subjects

THE PREVIOUS COHORT in which we originally analyzed the risk of liver stiffness for HCC development was employed; 866 chronic hepatitis C patients were enrolled between December 2004 and June 2005 at the Department of Gastroenterology, The University of Tokyo Hospital.[15] Among these patients, 112 patients, who had HCV genotype 1 and HCV RNA >100 KIU/mL, underwent PEG IFN plus RBV therapy after the enrollment. The potential association between PLNE and efficacy of PEG IFN plus RBV therapy was examined with these patients. When each subject was screened for HCC with ultrasonography at or immediately after the enrollment, the presence of PLNE was evaluated. The criteria to identify PLNE were previously described, and PLNE was defined as a lymph node at perihepatic area which was at least 1 cm in the longest axis.[10]

Moreover, between December 2011 and March 2012, 45 chronic hepatitis C patients with genotype 1 were enrolled at the Department of Gastroenterology, The University of Tokyo Hospital, to assess the potential association between PLNE and the known factors to predict the response to IFN therapy, namely, the mutations at position 70 of HCV core protein, those at IFN sensitivity-determining region (ISDR) of NS5A protein or interleukin (IL)-28B polymorphism.

The present study was carried out in accordance with the ethical guidelines of the Declaration of Helsinki and was approved by the Institutional Research Ethics Committee of the authors' institution. Informed consent was obtained for the use of the samples in this study.

Laboratory tests

Sequences of ISDR and the core region of HCV were determined by direct sequencing after amplification by reverse transcription and polymerase chain reaction as reported previously.[16,17] Genetic polymorphism in one tagging single nucleotide polymorphism located near the *IL-28B* gene (rs8099917) was determined by direct sequencing.[18] Homozygosity (GG) or heterozygosity (TG) of the minor sequence was defined as having the IL-28B minor allele, whereas homozygosity for the major sequence (TT) was defined as having the IL-28B major allele. Null virological response (NVR) was defined as detectable HCV RNA by qualitative polymerase chain reaction with a lower detection limit of 50 IU/mL (Amplicor; Roche Diagnostic Systems, Pleasanton, CA, USA) during the therapy. SVR was defined as undetectable HCV RNA 24 weeks after the completion of therapy. Relapse was defined as reappearance of HCV RNA after the completion of therapy. HCV RNA was quantitated using Amplicore HCV ver. 2.0 (Roche, Tokyo, Japan) or Cobas Ampliprep/Cobas TaqMan assay system (Roche, Tokyo, Japan). HCV genotype was determined based on the serotyping assay (SRL, Tokyo, Japan) or direct sequence analysis.[19]

Statistical analysis

Data were expressed as the mean ± standard deviation (SD) unless otherwise indicated. The categorical variables were compared by χ^2-test or Fischer's exact test, whereas continuous variables were compared by unpaired Student's *t*-test (parametric), Mann–Whitney *U*-test (non-parametric), Kruskal–Wallis rank sum test (non-parametric) or Wilcoxon rank sum test (non-parametric). For comparing group means, we used ANOVA. In the analysis of predicting factors for the responses to PEG IFN plus RBV therapy, the following

variables were tested in univariate and multivariate logistic regression analysis: age, sex, serum albumin, aspartate aminotransferase (AST), alanine aminotransferase (ALT), γ-glutamyltransferase (GGT), alkaline phosphatase, total bilirubin, α-fetoprotein (AFP) levels, prothrombin activity (%), liver stiffness values, platelet count, HCV viral load and the presence of PLNE. Factors that had a *P*-value of less than 0.4 in univariate analysis were subsequently included in multivariate logistic regression analysis. A *P*-value of less than 0.05 was considered significant. Data processing and analysis were performed using StatView ver. 5.0 (SAS Institute, Cary, NC, USA) and SPSS ver. 14.0 (SPSS, Chicago, IL, USA) software.

RESULTS

Association between PLNE and efficacy of PEG IFN plus RBV therapy

THE CLINICAL FEATURES of patients are summarized according to the presence or absence of PLNE in Table 1. All the patients were infected with HCV genotype 1 and had a high viral load (HCV RNA >100 KIU/mL). No patients were co-infected with hepatitis B virus. PLNE was observed in 22 of 112 (20.0%) patients analyzed.

PEG IFN-2a was administrated in 24 patients, while PEG IFN-2b in 88 patients. This ratio between patients treated with PEG IFN-2a and those with PEG IFN-2b was not different between patients with PLNE and those without (data not shown). Most of the patients were treated when the extended treatment of PEG IFN plus RBV therapy for more than 48 weeks was not generally performed in Japan; 27 of 112 (24.1%) patients received PEG IFN plus RBV for more than 48 weeks up to 72 weeks. After PEG IFN plus RBV therapy, SVR was achieved in 41 of 112 (36.6%) patients in this cohort. Between patients with PLNE and those without, the SVR rate was significantly lower in the former (4/22, 18.2%) than in the latter (37/90, 41.1%) ($P = 0.045$; Table 1). Of note, liver stiffness values as well as serum albumin levels, prothrombin activity and platelet count, which may be suggestive of liver fibrosis, were not different between patients with PLNE and those without (Table 1). Only serum GGT levels among the blood parameters were significantly lower in patients with PLNE than in those without.

To examine whether PLNE may influence virological response, the viral loads before treatment and at week 4 of treatment are depicted according to the presence or absence of PLNE in Figure 1. Viral decline between the start of treatment and week 4 was smaller in patients with PLNE than in those without ($P = 0.028$ by Wilcoxon rank sum test).

Patient characteristics according to the virological responses are shown in Table 2. In six patients, the

Table 1 Patient characteristics according to the presence or absence of PLNE

Parameter	PLNE positive, $n = 22$	PLNE negative, $n = 90$	*P*-value
Age (years)†	60.5 ± 8.8	57.2 ± 8.9	0.12
Male/female	14/8	40/50	0.10
Albumin (g/dL)†	4.01 ± 0.40	4.04 ± 0.33	0.75
AST (U/L)†	62.6 ± 41.2	61.0 ± 38.9	0.87
ALT (U/L)†	76.0 ± 62.2	72.4 ± 56.6	0.81
GGT (U/L)†	37.2 ± 24.6	53.5 ± 39.1	0.018
Alkaline phosphatase (U/L)†	211.7 ± 80.9	199.0 ± 66.3	0.50
Total bilirubin (mg/dL)†	0.82 ± 0.29	0.87 ± 0.47	0.48
Prothrombin time activity (%)	85.8 ± 12.5	85.9 ± 14.7	0.97
AFP (ng/mL)†	22.8 ± 44.0	13.0 ± 21.7	0.32
Liver stiffness (kPa)†	10.8 ± 6.9	12.7 ± 11.9	0.32
Platelet count ($\times 10^4/\mu L$)†	15.2 ± 8.2	15.5 ± 5.3	0.85
HCV viral load (KIU/mL)‡	731 (358–1070)	636 (151–1045)	0.51
SVR rate (%)§	18.2	41.1	0.045

†Data are presented as mean ± standard deviation, and compared by Student's *t*-tests.
‡Data are presented as median (25–75% range), and compared by Mann–Whitney *U*-tests.
§Data are compared by χ^2-tests.
AFP, α-fetoprotein; ALT, alanine aminotransferase; AST, aspartate aminotransferase; GGT, γ-glutamyltransferase; HCV, hepatitis C virus; IL, interleukin; PLNE, perihepatic lymph node enlargement; SVR, sustained virological response.

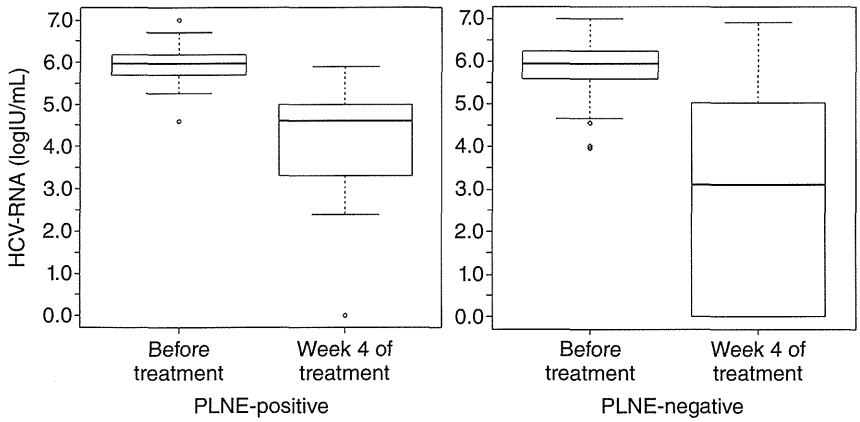

Figure 1 Changes in viral load in patients treated by PEG IFN plus RBV according to the presence or absence of PLNE. The viral loads before treatment with PEG IFN plus RBV and at week 4 of treatment were analyzed in patients with PLNE (PLNE positive, $n = 22$) and without PLNE (PLNE negative, $n = 90$). Viral decline was smaller in patients with PLNE than in those without ($P = 0.028$ by Wilcoxon rank sum test). HCV, hepatitis C virus; PEG IFN, pegylated interferon-α; PLNE, perihepatic lymph node enlargement; RBV, ribavirin.

effect of PEG IFN plus RBV therapy was lost during the treatment. Among the three groups of patients divided by the treatment outcome, namely, SVR, relapse or NVR, the rate of PLNE positive patients was least (4/41, 9.8%) in the SVR group ($P = 0.033$). Regarding other parameters, liver stiffness values were lowest ($P = 0.033$) in the SVR group, whereas serum albumin levels were lowest in the NVR group ($P = 0.004$), in line with the well-known evidence that patients with advanced liver fibrosis are difficult to treat with IFN.[20]

Then, the predicting factors for SVR were analyzed, and the results are shown in Table 3. Nine factors that had a *P*-value of less than 0.4 in univariate analysis were subsequently included in multivariate logistic regression analysis. As a result, ALT, GGT, liver stiffness and PLNE were retained as independent predicting factors for SVR (Table 3). These results suggest that the presence of PLNE is a negative predictor for achievement of SVR by PEG IFN and RBV therapy in chronic hepatitis C patients with genotype 1 and HCV RNA of more than 100 KIU/mL, independent of liver fibrosis.

Table 2 Patient characteristics according to the virological responses

Parameter	SVR, $n = 41$	Relapse, $n = 29$	NVR, $n = 36$	*P*-value
Age (years)†	57.3 ± 8.9	57.3 ± 9.1	58.8 ± 8.9	0.71
Male/female§	18/23	16/13	17/19	0.55
Albumin (g/dL)†	4.11 ± 0.28	4.10 ± 0.35	3.87 ± 0.37	0.004
AST (U/L)†	61.2 ± 43.8	56.6 ± 33.9	65.2 ± 34.1	0.67
ALT (U/L)†	81.6 ± 70.6	63.2 ± 40.1	71.4 ± 37.1	0.36
GGT (U/L)†	42.6 ± 30.3	48.5 ± 33.4	62.8 ± 45.6	0.056
Alkaline phosphatase (U/L)†	187.2 ± 73.9	211.7 ± 56.6	203.0 ± 73.7	0.33
Total bilirubin (mg/dL)†	0.78 ± 0.22	0.86 ± 0.32	0.99 ± 0.67	0.11
Prothrombin time (%)†	86.1 ± 17.1	84.8 ± 12.4	87.1 ± 12.3	0.80
AFP (ng/mL)†	9.6 ± 18.5	12.0 ± 27.0	23.2 ± 35.5	0.082
Liver stiffness (kPa)†	8.9 ± 4.7	13.5 ± 11.7	15.4 ± 14.9	0.033
Platelet counts ($\times 10^4/\mu L$)†	16.1 ± 4.4	16.8 ± 7.7	13.7 ± 5.8	0.077
HCV viral load (KIU/mL)‡	641 (150–1260)	670 (286–1168)	615 (168–951)	0.86
PLNE negative/positive§	37/4	21/8	28/8	0.033
Rate of PLNE positive (%)	9.8	27.6	22.2	

†Data are presented as mean ± standard deviation and compared by Student's *t*-tests.
‡Data are presented as median (25–75% range) and compared by Kruskal–Wallis rank sum tests.
§Data are compared by Fischer's exact tests.
AFP, α-fetoprotein; ALT, alanine aminotransferase; AST, aspartate aminotransferase; GGT, γ-glutamyltransferase; HCV, hepatitis C virus; IL, interleukin; NVR, null virological response; PLNE, perihepatic lymph node enlargement; SVR, sustained virological response.

Table 3 Univariate and multivariate analyses of contributing factors associated with SVR

Parameter	Univariate analysis, OR (95% CI), *P*-value	Multivariate analysis, OR (95% CI), *P*-value
Age (years)	0.989 (0.968–1.011), 0.619	
Male/female	1.314 (0.886–1.949), 0.488	
Albumin (g/dL)	2.547 (1.399–4.637), 0.119	1.702 (0.728–3.979), 0.531
AST (U/L)	0.999 (0.995–1.005), 0.982	
ALT (U/L)	1.004 (1.001–1.007), 0.250	1.015 (1.009–1.020), 0.005
GGT (U/L)	0.989 (0.983–0.996), 0.101	0.981 (0.973–0.989), 0.022
Alkaline phosphatase (U/L)	0.995 (0.996–0.998), 0.101	0.998 (0.995–1.002), 0.698
Total bilirubin (mg/dL)	0.335 (0.166–0.679), 0.121	0.475 (0.257–0.877), 0.225
Prothrombin time activity (%)	1.002 (0.988–1.016), 0.895	
AFP (ng/mL)	0.984 (0.972–0.995), 0.154	0.999 (0.979–1.020), 0.986
Liver stiffness (kPa)	0.917 (0.884–0.952), 0.019	0.866 (0.810–0.927), 0.033
Platelet ($\times 10^4/\mu L$)	1.030 (0.997–1.065), 0.366	0.958 (0.913–1.006), 0.381
HCV RNA viral load (KIU/mL)	0.850 (0.561–1.287), 0.695	
PLNE	0.318 (0.176–0.576), 0.053	0.179 (0.090–0.354), 0.012

AFP, α-fetoprotein; ALT, alanine aminotransferase; AST, aspartate aminotransferase; CI, confidence interval; GGT, γ-glutamyltransferase; HCV, hepatitis C virus; IL, interleukin; OR, odds ratio; PLNE, perihepatic lymph node enlargement; SVR, sustained virological response.

Association between PLNE and the mutations at position 70 of HCV core protein and at ISDR or IL-28B polymorphism

Recently, as a human factor, *IL-28B* polymorphism has been shown to be a strong predictor for the response to PEG IFN and RBV therapy for chronic hepatitis C.[21–23] On the other hand, as a viral factor, the mutations at position 70 of HCV core protein[24] and those at ISDR of NS5A protein[25] have been revealed to be associated with the treatment outcome by IFN. Thus, the potential associations between PLNE and these factors were evaluated. To this end, we first sought to analyze them in the original cohort, however, the stored samples were not enough for these determinations. Thus, we newly enrolled 45 chronic hepatitis C patients to only assess the potential associations between PLNE and *IL-28B* polymorphism, the mutations at position 70 of HCV core protein or those at ISDR of NS5A protein.

The clinical features of these 45 patients with chronic hepatitis C with HCV genotype 1 are summarized in Table 4. Among these patients, PLNE was observed in 18 patients (40%). Regarding *IL-28B* genotypes, the frequency of the rs8099917 risk allele (G), namely, minor allele, was not different between the patients with PLNE and those without: 22.2% in the former and 23.1% in the latter ($P = 0.76$ by χ^2-test; Fig. 2a). As a viral factor, the mutations at position 70 of HCV core protein were observed in 44.4% patients with PLNE, and in 42.3% patients without ($P = 0.87$ by χ^2-test; Fig. 2b), and less than two substitutions at ISDR were observed in 52.9% patients with PLNE, and in 64.0% patients without ($P = 0.69$ by χ^2-test; Fig. 2c), none of which were statistically different. These results suggest that PLNE is not associated with *IL-28B* polymorphism, or the mutations

Table 4 Characteristics of patients in whom the mutations at position 70 of HCV core protein and at ISDR or IL-28B polymorphism were measured

Parameter	$n = 45$
Age (years)†	68.1 ± 10.7
Male/female	19/26
Albumin (g/dL)†	3.93 ± 0.39
AST (U/L)†	43.4 ± 18.6
ALT (U/L)†	38.8 ± 20.3
GGT (U/L)†	38.1 ± 28.9
Alkaline phosphatase (U/L)†	276.3 ± 101.5
Total bilirubin (mg/dL)†	0.83 ± 0.29
Prothrombin time activity (%)	99.1 ± 2.86
AFP (ng/mL)†	16.0 ± 36.3
Platelet count ($\times 10^4/\mu L$)†	15.4 ± 7.0
HCV viral load (log IU/mL)‡	5.94 (5.54–6.60)
PLNE positive/negative	18/27

†Data are presented as mean ± standard deviation.
‡Data are presented as median (25–75% range).
AFP, α-fetoprotein; ALT, alanine aminotransferase; AST, aspartate aminotransferase; GGT, γ-glutamyltransferase; HCV, hepatitis C virus; IL, interleukin; ISDR, interferon sensitivity-determining region; PLNE, perihepatic lymph node enlargement;.

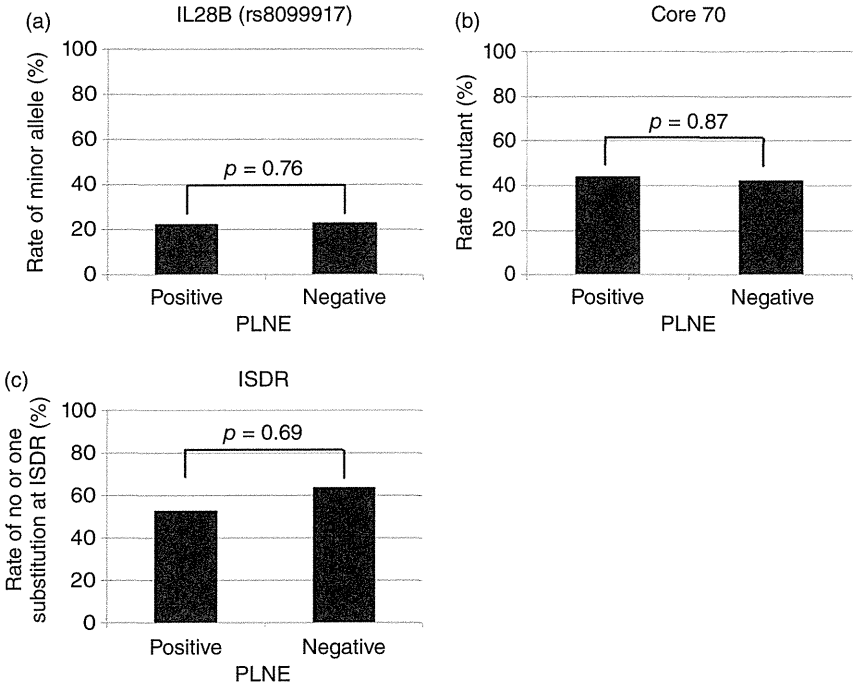

Figure 2 Rate of IL-28B minor allele (a), mutant at position 70 of HCV core protein (Core 70, b), and no or one substitution at ISDR (c) in patients with PLNE (positive) or without PLNE (negative). The rate of IL-28B minor allele (a), mutant at position 70 of HCV core protein (Core 70, b), and no or one substitutions at ISDR (c) was analyzed in patients with PLNE (positive, $n = 18$) or without PLNE (negative, $n = 27$). HCV, hepatitis C virus; IL, interleukin; ISDR, interferon sensitivity-determining region; PLNE, perihepatic lymph node enlargement.

at position 70 of HCV core protein and those at ISDR of NS5A protein.

DISCUSSION

THE FACT THAT chronic hepatitis C patients with PLNE are prone to treatment failure to IFN therapy has been previously reported.[10–12] However, there were limitations because these analyses were performed in patients with various HCV genotypes, viral loads and treatment regimens. It is well known that efficacy of IFN therapy for chronic hepatitis C is poorest in patients with HCV genotype 1 and higher HCV viral load.[13] On the other hand, IFN therapy has been refined with PEG and combination with RBV and protease inhibitors.[26] Thus, to more precisely examine the potential association between PLNE and efficacy of IFN therapy for chronic hepatitis C patients, we sought to analyze the efficacy of PEG IFN and RBV therapy on patients with HCV genotype 1 and HCV RNA of more than 100 KIU/mL in the presence or absence of PLNE. As a result, the SVR rate was significantly lower and the viral decline during the first 4 weeks of treatment was significantly smaller in patients with PLNE than in those without, and PLNE was negatively associated with SVR by multivariate analysis. It is noteworthy that PLNE was not associated with liver stiffness values, a marker of liver fibrosis,[27] although controversy exists whether PLNE may be associated with liver fibrosis,[2,4] and more importantly that PLNE was retained as a negative predictor for SVR by multivariate analysis, independent of liver fibrosis, in the current study.

To examine the underlying mechanism in the association between PLNE and efficacy of PEG IFN and RBV for chronic hepatitis C, we analyzed the potential links between PLNE and well-established host or viral factors to predict outcome by IFN therapy. We especially considered the possibility that PLNE may be associated with *IL-28B* polymorphism, which could be importantly involved in the host immune system.[21–23] However, PLNE was not significantly associated with *IL-28B* polymorphism as a host factor, in addition to no association of PLNE with the mutations at position 70 of HCV core protein[24] and those at ISDR[25] as a viral factor. Thus, we speculate that PLNE may reflect an unknown host factor to play a role in the reaction to HCV infection.

Perihepatic lymph node enlargement in chronic hepatitis C has long been assumed to reflect the immunological response of the host.[7] Indeed, higher $CD8^+$ lymphocyte levels in the blood were observed in chronic hepatitis C patients with PLNE,[7] and HCV-specific IFN-γ production and proliferative response of T cells were found commonly in perihepatic lymph node,[28] suggesting that PLNE indicates an active host immune response

in chronic hepatitis C. Of interest is the finding that biochemical responders to IFN-α therapy for chronic hepatitis C had significantly lower pretreatment levels of $CD8^+$ cells.[29] Thus, increased $CD8^+$ cell levels in chronic hepatitis C patients with PLNE[7] may explain the mechanism, at least in part, of the association between PLNE and the poorer outcome by PEG IFN and RBV therapy. Furthermore, increased oligoclonality of circulating $CD8^+$ cells in chronic HCV infection was also identified as an indicator for poor clinical response to IFN-α therapy.[30] It should be further clarified whether the altered clonality of $CD8^+$ cells may be also involved in the mechanism of the association between PLNE and the efficacy of PEG IFN and RBV therapy.

We previously demonstrated that PLNE is a negative risk for hepatocarcinogenesis in chronic hepatitis C.[10] Currently, we have found that PLNE is a negative predictor for a successful outcome of IFN treatment for chronic hepatitis C, both of which could be paradoxical. However, these findings may be consistently explained by an active host immune system as described above. We previously speculated that the reduced hepatocarcinogenesis in chronic hepatitis C patients with PLNE may be explained by the enhanced host immune system. On the other hand, there are accumulating lines of evidence suggesting that the originally enhanced host immune response may be associated with a negative outcome of IFN treatment for chronic hepatitis C; the higher expression of IFN-stimulated genes in the liver was observed in patients with no response to IFN treatment for chronic hepatitis C.[31–35] Thus, we speculate that PLNE, as an indicator of active host immune responses,[7,28] may be associated negatively with the efficacy of IFN therapy for chronic hepatitis C in line with these previous studies.

One of the limitations of the current study is that the association between PLNE and efficacy of IFN therapy in chronic hepatitis C patients was determined in the retrospective cohort. However, the cohort analyzed was originally set up to prospectively examine the risk of liver stiffness values for HCC development, where patients were consecutively enrolled among those who previously visited our Department of Gastroenterology, The University of Tokyo Hospital,[15] and were followed up for 4.8 years.[10] Thus, we believe that our current evidence could be the same as that from the prospective cohort. As another limitation, the association between PLNE and *IL-28B* polymorphism, the mutations at position 70 of HCV core protein or those at ISDR could not be assessed in the original cohort, because the stored samples of the original cohort were not enough for these determinations.

The combination of PEG IFN and RBV has been the standard of care for chronic hepatitis C,[26] and the further combination of telaprevir[36] or boceprevir[37] with PEG IFN and RBV has been recently employed to improve the treatment efficacy. Nonetheless, it is expected that IFN is still going to play a role in the treatment for chronic hepatitis C. Thus, our evidence of PLNE as a significant predictor for SVR by PEG IFN and RBV therapy may be useful when deciding upon the regimen or timing treatment for chronic hepatitis C patients. Furthermore, because PLNE is originally one of the common clinical signs of chronic liver disease,[1–3] the knowledge regarding the clinical significance of PLNE may shed a light on not only the prediction of treatment outcome of IFN therapy for chronic hepatitis C but also the general pathophysiology of chronic liver disease.

REFERENCES

1 Cassani F, Zoli M, Baffoni L *et al.* Prevalence and significance of abdominal lymphadenopathy in patients with chronic liver disease: an ultrasound study. *J Clin Gastroenterol* 1990; **12**: 42–6.
2 Cassani F, Valentini P, Cataleta M *et al.* Ultrasound-detected abdominal lymphadenopathy in chronic hepatitis C: high frequency and relationship with viremia. *J Hepatol* 1997; **26**: 479–83.
3 Dietrich CF, Lee JH, Herrmann G *et al.* Enlargement of perihepatic lymph nodes in relation to liver histology and viremia in patients with chronic hepatitis C. *Hepatology* 1997; **26**: 467–72.
4 Soresi M, Carroccio A, Agate V *et al.* Evaluation by ultrasound of abdominal lymphadenopathy in chronic hepatitis C. *Am J Gastroenterol* 1999; **94**: 497–501.
5 Zhang XM, Mitchell DG, Shi H *et al.* Chronic hepatitis C activity: correlation with lymphadenopathy on MR imaging. *AJR Am J Roentgenol* 2002; **179**: 417–22.
6 del Olmo JA, Esteban JM, Maldonado L *et al.* Clinical significance of abdominal lymphadenopathy in chronic liver disease. *Ultrasound Med Biol* 2002; **28**: 297–301.
7 Muller P, Renou C, Harafa A *et al.* Lymph node enlargement within the hepatoduodenal ligament in patients with chronic hepatitis C reflects the immunological cellular response of the host. *J Hepatol* 2003; **39**: 807–13.
8 Watanabe T, Sassa T, Hiratsuka H, Hattori S, Abe A. Clinical significance of enlarged perihepatic lymph node on ultrasonography. *Eur J Gastroenterol Hepatol* 2005; **17**: 185–90.
9 Tavakoli-Tabasi S, Ninan S. Clinical significance of perihepatic lymphadenopathy in patients with chronic hepatitis C infection. *Dig Dis Sci* 2011; **56**: 2137–44.
10 Hikita H, Nakagawa H, Tateishi R *et al.* Perihepatic lymph node enlargement is a negative predictor of liver cancer

development in chronic hepatitis C patients. *J Gastroenterol.* Epub ahead of print: DOI 10.1007/s00535-012-0635-7.
11 Dietrich CF, Stryjek-Kaminska D, Teuber G, Lee JH, Caspary WF, Zeuzem S. Perihepatic lymph nodes as a marker of antiviral response in patients with chronic hepatitis C infection. *AJR Am J Roentgenol* 2000; **174**: 699–704.
12 Soresi M, Bonfissuto G, Sesti R *et al.* Perihepatic lymph nodes and antiviral response in chronic HCV-associated hepatitis. *Ultrasound Med Biol* 2004; **30**: 711–17.
13 Shiratori Y, Kato N, Yokosuka O *et al.* Predictors of the efficacy of interferon therapy in chronic hepatitis C virus infection. Tokyo-Chiba Hepatitis Research Group. *Gastroenterology* 1997; **113**: 558–66.
14 Manns MP, McHutchison JG, Gordon SC *et al.* Peginterferon alfa-2b plus ribavirin compared with interferon alfa-2b plus ribavirin for initial treatment of chronic hepatitis C: a randomised trial. *Lancet* 2001; **358**: 958–65.
15 Masuzaki R, Tateishi R, Yoshida H *et al.* Prospective risk assessment for hepatocellular carcinoma development in patients with chronic hepatitis C by transient elastography. *Hepatology* 2009; **49**: 1954–61.
16 Ibarrola N, Moreno-Monteagudo JA, Saiz M *et al.* Response to retreatment with interferon-alpha plus ribavirin in chronic hepatitis C patients is independent of the NS5A gene nucleotide sequence. *Am J Gastroenterol* 1999; **94**: 2487–95.
17 Hayashi K, Katano Y, Ishigami M *et al.* Mutations in the core and NS5A region of hepatitis C virus genotype 1b and correlation with response to pegylated-interferon-alpha 2b and ribavirin combination therapy. *J Viral Hepat* 2011; **18**: 280–6.
18 Akkarathamrongsin S, Sugiyama M, Matsuura K *et al.* High sensitivity assay using serum sample for IL28B genotyping to predict treatment response in chronic hepatitis C patients. *Hepatol Res* 2010; **40**: 956–62.
19 Gargiulo F, De Francesco MA, Pinsi G *et al.* Determination of HCV genotype by direct sequence analysis of quantitative PCR products. *J Med Virol* 2003; **69**: 202–6.
20 Tsubota A, Chayama K, Ikeda K *et al.* Factors predictive of response to interferon-alpha therapy in hepatitis C virus infection. *Hepatology* 1994; **19**: 1088–94.
21 Ge D, Fellay J, Thompson AJ *et al.* Genetic variation in IL28B predicts hepatitis C treatment-induced viral clearance. *Nature* 2009; **461**: 399–401.
22 Tanaka Y, Nishida N, Sugiyama M *et al.* Genome-wide association of IL28B with response to pegylated interferon-alpha and ribavirin therapy for chronic hepatitis C. *Nat Genet* 2009; **41**: 1105–9.
23 Suppiah V, Moldovan M, Ahlenstiel G *et al.* IL28B is associated with response to chronic hepatitis C interferon-alpha and ribavirin therapy. *Nat Genet* 2009; **41**: 1100–4.
24 Akuta N, Suzuki F, Sezaki H *et al.* Association of amino acid substitution pattern in core protein of hepatitis C virus genotype 1b high viral load and non-virological response to interferon-ribavirin combination therapy. *Intervirology* 2005; **48**: 372–80.
25 Enomoto N, Sakuma I, Asahina Y *et al.* Comparison of full-length sequences of interferon-sensitive and resistant hepatitis C virus 1b. Sensitivity to interferon is conferred by amino acid substitutions in the NS5A region. *J Clin Invest* 1995; **96**: 224–30.
26 Afdhal NH, McHutchison JG, Zeuzem S *et al.* Hepatitis C pharmacogenetics: state of the art in 2010. *Hepatology* 2011; **53**: 336–45.
27 Castera L, Vergniol J, Foucher J *et al.* Prospective comparison of transient elastography, Fibrotest, APRI, and liver biopsy for the assessment of fibrosis in chronic hepatitis C. *Gastroenterology* 2005; **128**: 343–50.
28 Moonka D, Milkovich KA, Rodriguez B, Abouljoud M, Lederman MM, Anthony DD. Hepatitis C virus-specific T-cell gamma interferon and proliferative responses are more common in perihepatic lymph nodes than in peripheral blood or liver. *J Virol* 2008; **82**: 11742–8.
29 Saito H, Ebinuma H, Satoh I *et al.* Immunological and virological predictors of outcome during interferon-alpha therapy of chronic hepatitis C. *J Viral Hepat* 2000; **7**: 64–74.
30 Manfras BJ, Weidenbach H, Beckh KH *et al.* Oligoclonal CD8+ T-cell expansion in patients with chronic hepatitis C is associated with liver pathology and poor response to interferon-alpha therapy. *J Clin Immunol* 2004; **24**: 258–71.
31 Chen L, Borozan I, Feld J *et al.* Hepatic gene expression discriminates responders and nonresponders in treatment of chronic hepatitis C viral infection. *Gastroenterology* 2005; **128**: 1437–44.
32 Feld JJ, Nanda S, Huang Y *et al.* Hepatic gene expression during treatment with peginterferon and ribavirin: identifying molecular pathways for treatment response. *Hepatology* 2007; **46**: 1548–63.
33 Sarasin-Filipowicz M, Oakeley EJ, Duong FH *et al.* Interferon signaling and treatment outcome in chronic hepatitis C. *Proc Natl Acad Sci U S A* 2008; **105**: 7034–9.
34 Asselah T, Bieche I, Narguet S *et al.* Liver gene expression signature to predict response to pegylated interferon plus ribavirin combination therapy in patients with chronic hepatitis C. *Gut* 2008; **57**: 516–24.
35 Honda M, Sakai A, Yamashita T *et al.* Hepatic ISG expression is associated with genetic variation in interleukin 28B and the outcome of IFN therapy for chronic hepatitis C. *Gastroenterology* 2010; **139**: 499–509.
36 Jacobson IM, McHutchison JG, Dusheiko G *et al.* Telaprevir for previously untreated chronic hepatitis C virus infection. *N Engl J Med* 2011; **364**: 2405–16.
37 Poordad F, McCone J, Jr, Bacon BR *et al.* Boceprevir for untreated chronic HCV genotype 1 infection. *N Engl J Med* 2011; **364**: 1195–206.

Cell

Identification of Liver Cancer Progenitors Whose Malignant Progression Depends on Autocrine IL-6 Signaling

Guobin He,[1,13] Debanjan Dhar,[1,13] Hayato Nakagawa,[1,11,13] Joan Font-Burgada,[1,13] Hisanobu Ogata,[1,12,13] Yuhong Jiang,[1] Shabnam Shalapour,[1] Ekihiro Seki,[2] Shawn E. Yost,[4,5] Kristen Jepsen,[5] Kelly A. Frazer,[5,6,7,8] Olivier Harismendy,[5,6,7] Maria Hatziapostolou,[9] Dimitrios Iliopoulos,[9] Atsushi Suetsugu,[3,10] Robert M. Hoffman,[3,10] Ryosuke Tateishi,[11] Kazuhiko Koike,[11] and Michael Karin[1,6,*]

[1]Laboratory of Gene Regulation and Signal Transduction, Departments of Pharmacology and Pathology
[2]Department of Medicine
[3]Department of Surgery
[4]Bioinformatics Graduate Program
[5]Rady's Children's Hospital and Department of Pediatrics
[6]Moores UCSD Cancer Center
[7]Clinical and Translational Research Institute
[8]Institute for Genomic Medicine
University of California San Diego, School of Medicine, 9500 Gilman Drive, San Diego, CA 92093, USA
[9]Center for Systems Biomedicine, Division of Digestive Diseases and Institute for Molecular Medicine, David Geffen School of Medicine, University of California Los Angeles, Los Angeles, CA 90095, USA
[10]AntiCancer, Inc., San Diego, CA 92111, USA
[11]Department of Gastroenterology, University of Tokyo, Tokyo 113-8655, Japan
[12]Department of Medicine and Clinical Science, Graduate School of Medical Sciences, Kyushu University, Fukuoka 812-8582, Japan
[13]These authors contributed equally to this work
*Correspondence: karinoffice@ucsd.edu
http://dx.doi.org/10.1016/j.cell.2013.09.031

SUMMARY

Hepatocellular carcinoma (HCC) is a slowly developing malignancy postulated to evolve from premalignant lesions in chronically damaged livers. However, it was never established that premalignant lesions actually contain tumor progenitors that give rise to cancer. Here, we describe isolation and characterization of HCC progenitor cells (HcPCs) from different mouse HCC models. Unlike fully malignant HCC, HcPCs give rise to cancer only when introduced into a liver undergoing chronic damage and compensatory proliferation. Although HcPCs exhibit a similar transcriptomic profile to bipotential hepatobiliary progenitors, the latter do not give rise to tumors. Cells resembling HcPCs reside within dysplastic lesions that appear several months before HCC nodules. Unlike early hepatocarcinogenesis, which depends on paracrine IL-6 production by inflammatory cells, due to upregulation of LIN28 expression, HcPCs had acquired autocrine IL-6 signaling that stimulates their in vivo growth and malignant progression. This may be a general mechanism that drives other IL-6-producing malignancies.

INTRODUCTION

Every malignant tumor is probably derived from a single progenitor that had acquired growth and survival advantages through genetic and epigenetic changes, allowing clonal expansion (Nowell, 1976). Tumor progenitors are not necessarily identical to cancer stem cells (CSCs), which maintain and renew fully established malignancies (Nguyen et al., 2012). However, clonal evolution and selective pressure may cause some descendants of the initial progenitor to cross the bridge of no return and form a premalignant lesion. Cancer genome sequencing indicates that most cancers require at least five genetic changes to evolve (Wood et al., 2007). How these changes affect the properties of tumor progenitors and control their evolution into a CSC is not entirely clear, as it has been difficult to isolate and propagate cancer progenitors prior to detection of tumor masses. Given these difficulties, it is also not clear whether cancer progenitors are the precursors for the more malignant CSC isolated from fully established cancers. An answer to these critical questions depends on identification and isolation of cancer progenitors, which may also enable definition of molecular markers and signaling pathways suitable for early detection and treatment. This is especially important in cancers of the liver and pancreas, which evolve over the course of many years but, once detected, are extremely difficult to treat (El-Serag, 2011; Hruban et al., 2007).

Hepatocellular carcinoma (HCC), the most common liver cancer, is the end product of chronic liver diseases, requiring

several decades to evolve (El-Serag, 2011). Currently, HCC is the third most deadly and fifth most common cancer worldwide, and in the United States its incidence has doubled in the past two decades. Furthermore, 8% of the world's population are chronically infected with hepatitis B or C viruses (HBV and HCV) and are at a high risk of new HCC development (El-Serag, 2011). Up to 5% of HCV patients will develop HCC in their lifetime, and the yearly HCC incidence in patients with cirrhosis is 3%–5%. These tumors may arise from premalignant lesions, ranging from dysplastic foci to dysplastic hepatocyte nodules that are often seen in damaged and cirrhotic livers and are more proliferative than the surrounding parenchyma (Hytiroglou et al., 2007). However, the tumorigenic potential of these lesions was never examined, and it is unknown whether they contain any genetic alterations. Given that there is no effective treatment for HCC and, upon diagnosis, most patients with advanced disease have a remaining lifespan of 4–6 months, it is important to detect HCC early, while it is still amenable to surgical resection or chemotherapy. Premalignant lesions, called foci of altered hepatocytes (FAH), were also described in chemically induced HCC models (Pitot, 1990), but it was questioned whether these lesions harbor tumor progenitors or result from compensatory proliferation (Sell and Leffert, 2008). The aim of this study was to determine whether HCC progenitor cells (HcPCs) exist and if so, to isolate these cells and identify some of the signaling networks that are involved in their maintenance and progression.

We now describe HcPC isolation from mice treated with the procarcinogen diethyl nitrosamine (DEN), which induces poorly differentiated HCC nodules within 8 to 9 months (Verna et al., 1996). Although these tumors do not evolve in the context of cirrhosis, the use of a chemical carcinogen is justified because the finding of up to 121 mutations per HCC genome suggests that carcinogens may be responsible for human HCC induction (Guichard et al., 2012). Furthermore, 20%–30% of HCC, especially in HBV-infected individuals, evolve in noncirrhotic livers (El-Serag, 2011). Nonetheless, we also isolated HcPCs from *Tak1*$^{\Delta hep}$ mice, which develop spontaneous HCC as a result of progressive liver damage, inflammation, and fibrosis caused by ablation of TAK1 (Inokuchi et al., 2010). Although the etiology of each model is distinct, both contain HcPCs that express marker genes and signaling pathways previously identified in human HCC stem cells (Marquardt and Thorgeirsson, 2010) long before visible tumors are detected. Furthermore, DEN-induced premalignant lesions and HcPCs exhibit autocrine IL-6 production that is critical for tumorigenic progression. Circulating IL-6 is a risk indicator in several human pathologies and is strongly correlated with adverse prognosis in HCC and cholangiocarcinoma (Porta et al., 2008; Soresi et al., 2006). IL-6 produced by in-vitro-induced CSCs was suggested to be important for their maintenance (Iliopoulos et al., 2009). Furthermore, autocrine IL-6 was detected in several cancers, but its origin is poorly understood (Grivennikov and Karin, 2008). In particular, little is known about the source of IL-6 in HCC. In early stages of hepatocarcinogenesis, IL-6 is produced by Kupffer cells or macrophages (Maeda et al., 2005; Naugler et al., 2007). However, paracrine IL-6 production is transient and does not explain its expression by HCC cells.

RESULTS

DEN-Induced Collagenase-Resistant Aggregates of HCC Progenitors

A single intraperitoneal (i.p.) injection of DEN into 15-day-old BL/6 mice induces HCC nodules first detected 8 to 9 months later. However, hepatocytes prepared from macroscopically normal livers 3 months after DEN administration already contain cells that progress to HCC when transplanted into the permissive liver environment of MUP-uPA mice (He et al., 2010), which express urokinase plasminogen activator (uPA) from a mouse liver-specific major urinary protein (MUP) promoter and undergo chronic liver damage and compensatory proliferation (Rhim et al., 1994). Collagenase digestion of DEN-treated livers generated a mixture of monodisperse hepatocytes and aggregates of tightly packed small hepatocytic cells (Figure 1A). Aggregated cells were also present—but in lower abundance—in digests of control livers (Figure S1A available online). HCC markers such as α fetoprotein (AFP), glypican 3 (Gpc3), and Ly6D, whose expression in mouse liver cancer was reported (Meyer et al., 2003), were upregulated in aggregates from DEN-treated livers, but not in nonaggregated hepatocytes or aggregates from control livers (Figure S1A). Thus, control liver aggregates may result from incomplete collagenase digestion, whereas aggregates from DEN-treated livers may contain HcPC. DEN-induced aggregates became larger and more abundant 5 months after carcinogen exposure, when they consisted of 10–50 cells that were smaller than nonaggregated hepatocytes. Using 70 μm and 40 μm sieves, we separated aggregated from nonaggregated hepatocytes (Figure 1A) and tested their tumorigenic potential by transplantation into MUP-uPA mice (Figure 1B). To facilitate transplantation, the aggregates were mechanically dispersed and suspended in Dulbecco's modified Eagle's medium (DMEM). Five months after intrasplenic (i.s.) injection of 10^4 viable cells, mice receiving cells from aggregates developed about 18 liver tumors per mouse, whereas mice receiving nonaggregated hepatocytes developed less than 1 tumor each (Figure 1B). The tumors exhibited typical trabecular HCC morphology and contained cells that abundantly express AFP (Figure S1B). To confirm that the HCCs were derived from transplanted cells, we measured their relative MUP-uPA DNA copy number and found that they contained much less MUP-uPA transgene DNA than the surrounding parenchyma (Figure S1C). Transplantation of aggregated cells from livers of DEN-treated actin-GFP transgenic mice resulted in GFP-positive HCCs (Figure S1D). Both experiments strongly suggest that the HCCs were derived from the transplanted cells. No tumors were ever observed after transplantation of control hepatocytes (nonaggregated or aggregated).

Only liver tumors were formed by the transplanted cells. Other organs, including the spleen into which the cells were injected, remained tumor free (Figure 1B), suggesting that HcPCs progress to cancer only in the proper microenvironment. Indeed, no tumors appeared after HcPC transplantation into normal BL/6 mice. But, if BL/6 mice were first treated with retrorsine (a chemical that permanently inhibits hepatocyte proliferation [Laconi et al., 1998]), intrasplenically transplanted with HcPC-containing aggregates, and challenged with CCl_4 to induce liver injury and compensatory proliferation (Guo et al., 2002), HCCs readily

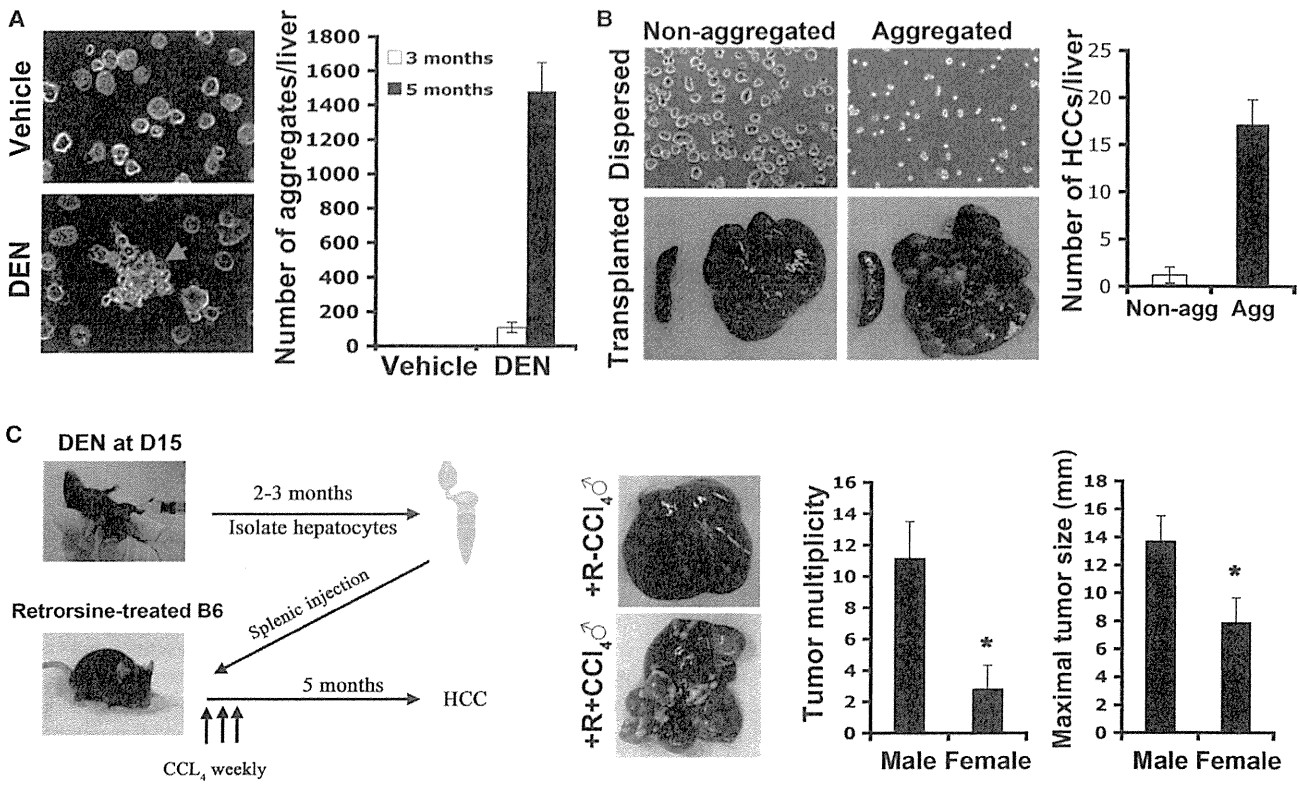

E

Type of cells	Number of cells transplanted			
	$4x10^4$	$1X10^4$	1000	100
Unsorted	2(2)	9(9)	2(5)	0(3)
$CD44^+$	nd	nd	4(4)	2(4)
$CD44^-$	nd	nd	0(4)	0(5)

Figure 1. DEN-Induced Hepatocytic Aggregates Contain $CD44^+$ HCC Progenitors

(A) Fifteen-day-old BL/6 males were given DEN or vehicle. After 3 or 5 months, their livers were removed and collagenase digested. Left: typical digest appearance (magnification: 400×; 3 months after DEN). Red arrow indicates a collagenase-resistant aggregate. Right: aggregates per liver (n = 5; ± SD for each point).

(B) Livers were collagenase digested 5 months after DEN administration. Aggregates were separated from nonaggregated cells and mechanically dispersed into a single-cell suspension (left upper panels; 200×). 10^4 viable aggregated or nonaggregated cells were i.s. injected into MUP-uPA mice whose livers and spleens were analyzed for tumors 5 months later (left lower panels). The number of HCC nodules per liver was determined (n = 5; ± SD).

(C) Adult BL/6 mice were given retrorsine twice with a 2 week interval to inhibit hepatocyte proliferation. After 1 month, mice were i.s. transplanted with dispersed hepatocyte aggregates (10^4 cells) from DEN-treated mice and, 2 weeks later, were given three weekly i.p. injections of CCl_4 or vehicle. Tumor multiplicity and size were evaluated 5 months later (n = 5; ± SD).

(D) Hepatocyte aggregates were prepared as in (A), stained with CD44 antibody and DAPI, and examined by fluorescent microscopy (400×).

(E) Hepatocyte aggregates were dispersed as above, and $CD44^+$ cells were separated from $CD44^-$ cells. The indicated cell numbers were injected into MUP-uPA mice, and HCC development was evaluated 5 months later. n values are in parentheses (n.d., not done).

See also Figure S1.

appeared (Figure 1C). CCl_4 omission prevented tumor development. Notably, MUP-uPA or CCl_4-treated livers are fragile, rendering direct intrahepatic transplantation difficult. The transplanted HcPC-containing aggregates formed more numerous and larger HCC nodules in male recipients than in females (Figure 1C), as observed in MUP-uPA mice transplanted with unfractionated DEN-exposed hepatocytes (He et al., 2010). Thus, CCl_4-induced liver damage, especially within a male liver, generates a microenvironment that drives HcPC proliferation and malignant progression. To examine this point, we transplanted GFP-labeled HcPC-containing aggregates into retrorsine-treated BL/6 mice and examined their ability to proliferate with or without subsequent CCl_4 treatment. Indeed, the GFP^+ cells formed clusters that grew in size only in CCl_4-treated host livers

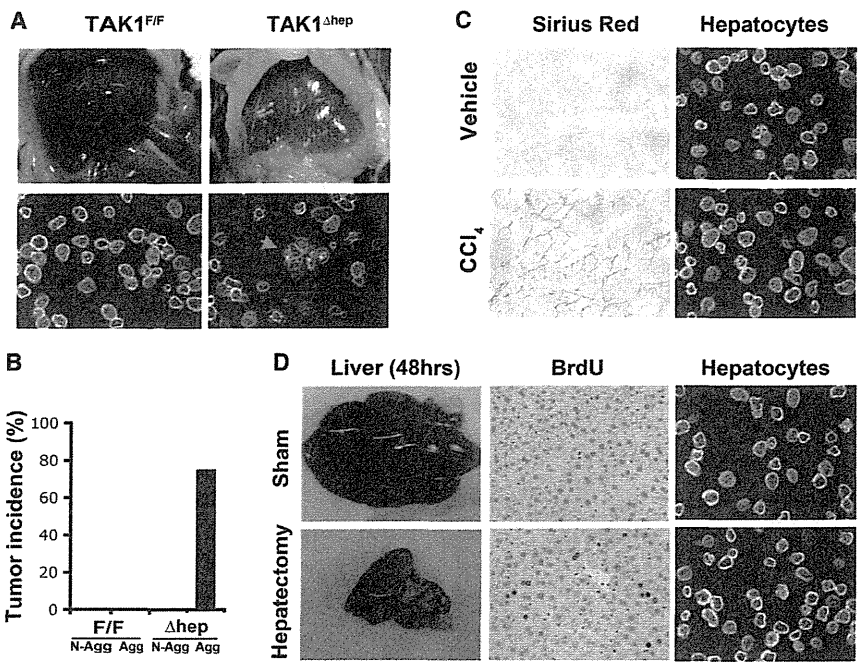

Figure 2. *Tak1*$^{\Delta hep}$ Livers Contain Collagenase-Resistant HcPC Aggregates

(A) Livers, free of tumors (upper panels), were removed from 1-month-old *Tak1*$^{F/F}$ and *Tak1*$^{\Delta hep}$ males and collagenase digested (lower panels; red arrow indicates collagenase-resistant aggregate).

(B) 10^4 nonaggregated or dispersed aggregated hepatocytes from (A) were i.s. injected into MUP-uPA mice that were analyzed 6 months later to identify mice with at least one liver tumor (n = 5–8 mice per genotype).

(C) BL/6 males were injected with vehicle or CCl_4 twice weekly for 2 weeks. Hepatocytes were isolated by collagenase digestion and photographed (right panels; 400×). Liver sections were stained with Sirius red to reveal collagen deposits (left panels).

(D) 8-week-old BL/6 males were subjected to 70% partial hepatectomy, pulsed with BrdU at 46 and 70 hr, and sacrificed 2 hr later. Isolated hepatocytes were photographed. Liver sections were analyzed for BrdU incorporation (400×). See also Figure S2 and Table S1.

(Figure S1E). Omission of CCl_4 prevented their expansion. Unlike HCC-derived cancer cells (dih10 cells), which form subcutaneous (s.c.) tumors with HCC morphology (He et al., 2010; Park et al., 2010), the HcPC-containing aggregates did not generate s.c. tumors in BL/6 mice (Figure S1F).

Despite their homogeneous appearance, the HcPC-containing aggregates contained both $CD44^+$ and $CD44^-$ cells (Figure 1D). Because CD44 is expressed by HCC stem cells (Yang et al., 2008; Zhu et al., 2010), we dispersed the aggregates and separated $CD44^+$ from $CD44^-$ cells and transplanted both into MUP-uPA mice. Whereas as few as 10^3 $CD44^+$ cells gave rise to HCCs in 100% of recipients, no tumors were detected after transplantation of $CD44^-$ cells (Figure 1E). Remarkably, 50% of recipients developed at least one HCC after receiving as few as 10^2 $CD44^+$ cells. Mature $CD44^-$ hepatocytes were found to engraft as well as or better than $CD44^+$ small hepatocytic cells (Haridass et al., 2009; Ichinohe et al., 2012). Hence, livers of DEN-treated mice contain $CD44^+$ HcPC that can be successfully isolated and purified and give rise to HCCs after transplantation into appropriate hosts. Unlike fully transformed HCC cells, HcPCs only give rise to tumors within the liver.

HcPC-Containing Aggregates in *Tak1*$^{\Delta hep}$ Mice

We applied the same HcPC isolation protocol to *Tak1*$^{\Delta hep}$ mice, which develop HCC of different etiology from DEN-induced HCC. Importantly, *Tak1*$^{\Delta hep}$ mice develop HCC as a consequence of chronic liver injury and fibrosis without carcinogen or toxicant exposure (Inokuchi et al., 2010). Indeed, whole-tumor exome sequencing revealed that DEN-induced HCC contained about 24 mutations per 10^6 bases (Mb) sequenced, with *B-Raf*^{V637E} being the most recurrent, whereas 1.4 mutations per Mb were detected in *Tak1*$^{\Delta hep}$ HCC's exome (Table S1). By contrast, *Tak1*$^{\Delta hep}$ HCC exhibited gene copy number changes.

Collagenase digests of 1-month-old *Tak1*$^{\Delta hep}$ livers contained much more hepatocytic aggregates than *Tak1*$^{f/f}$ liver digests (Figure 2A). Notably, HCC developed in 75% of MUP-uPA mice that received dispersed *Tak1*$^{\Delta hep}$ aggregates, but no tumors appeared in mice receiving nonaggregated *Tak1*$^{\Delta hep}$ or total *Tak1*$^{f/f}$ hepatocytes (Figure 2B). Because *Tak1*$^{\Delta hep}$ mice are subject to chronic liver damage and consequent compensatory proliferation, we wanted to ascertain that the HcPCs are not simply proliferating hepatocytes or expanding bipotential hepatobiliary progenitors using CCl_4 to induce liver injury and compensatory proliferation in WT mice. Although this treatment caused acute liver fibrosis, it did not augment formation of collagenase-resistant aggregates (Figure 2C). Similarly, few aggregates were detected in collagenase digests of livers after partial hepatectomy (Figure 2D). However, bile duct ligation (BDL) or feeding with 3,5-dicarbethoxy-1,4-dihydrocollidine (DDC), treatments that cause cholestatic liver injuries and oval cell expansion (Dorrell et al., 2011), did increase the number of small hepatocytic cell aggregates (Figure S2A). Nonetheless, no tumors were observed 5 months after injection of such aggregates into MUP-uPA mice (Figure S2B). Thus, not all hepatocytic aggregates contain HcPCs, and HcPCs only appear under tumorigenic conditions.

The HcPC Transcriptome Is Similar to that of HCC and Oval Cells

To determine the relationship between DEN-induced HcPCs, normal hepatocytes, and fully transformed HCC cells, we analyzed the transcriptomes of aggregated and nonaggregated hepatocytes from male littermates 5 months after DEN administration, HCC epithelial cells from DEN-induced tumors, and normal hepatocytes from age- and gender-matched littermate controls. Clustering analysis distinguished the HCC samples from other samples and revealed that the aggregated